Aging impact on sources, volatility, and viscosity of organic aerosols in the Chinese outflows

Tingting Feng[1,2,3,4,5&], Yingkun Wang[1,2,3,4,5&], Weiwei Hu[1,2,4,5,6*], Ming Zhu[1,2,3,4,5], Wei Song[1,2,4,5], Wei Chen[1,2,3,4,5], Yanyan Sang[7], Zheng Fang[1,2,3,4,5], Wei Deng[1,2,3,4,5], Hua Fang[1,2,3,4,5#], Xu Yu[1,2,3,4,5], Cheng Wu[8], Bin Yuan[9], Shan Huang[9], Min Shao[9], Xiaofeng Huang[10], Lingyan He[10], Young Ro Lee[11], L. Gregory Huey[11], Francesco Canonaco[12,13], Andre S. H. Prevot[12] , Xinming Wang[1,2,3,4,5]

[1]State Key Laboratory of Organic Geochemistry, Guangzhou Institute of Geochemistry, Chinese Academy of Sciences, Guangzhou 510640, China
[2]CAS Center for Excellence in Deep Earth Science, Guangzhou 510640, China
[3]Chinese Academy of Sciences University, Beijing 100049, China
[4]Guangdong-Hong Kong-Macao, Joint Laboratory for Environmental Pollution and Control, Guangzhou Institute of Geochemistry, Chinese Academy of Science, Guangzhou 510640, China
[5]Guangdong Provincial Key Laboratory of Environmental Protection and Resources Utilization, Chinese Academy of Science, Guangzhou 510640, China
[6]Shanghai Academy of Environmental Sciences, Shanghai 200233, China
[7]Tai'an Environmental Protection Bureau, Tai'an, Shandong 271000, China
[8]Institute of Mass Spectrometry and Atmospheric Environment, Jinan University, Guangzhou 510632, China
[9]Institute for Environmental and Climate Research, Jinan University, Guangzhou 511443, China
[10] Key Laboratory for Urban Habitat Environmental Science and Technology, School of Environment and Energy, Peking University Shenzhen Graduate School, Shenzhen, China
[11]School of Earth and Atmospheric Sciences, Georgia Institute of Technology, Atlanta, GA 30332, USA.
[12]Paul Scherrer Institute, Laboratory of Atmospheric Chemistry, 5232 Villigen PSI, Switzerland
[13]Datalystica Ltd., Park innovAARE, 5234 Villigen, Switzerland
#Now at School of Ecology and Environment, Anhui Normal University, Wuhu, Anhui 241000, China
&These authors contributed equally to this work and should be considered co-first authors.

*Correspondence: Weiwei Hu (weiweihu@gig.ac.cn)

Abstract. To investigate the aging impact on sources, volatility, and viscosity of organic aerosols (OA) in the Chinese outflows, a high-resolution time-of-flight aerosol mass spectrometer (HR-AMS) coupled with a thermodenuder (TD) was deployed in the spring of 2018 in Dongying, which is a regional receptor site of metropolitan emissions in North China Plain (NCP). The average mass concentration of PM_1 was 31.5 ± 22.7 μg m^{-3}, which was mainly composed of nitrate (33 %) and OA (25 %). The source apportionment results show the OA was mainly contributed by oxygenated OA (OOA) from secondary sources, including background-OOA (33 %) representing a background concentration of OA (2.6 μg m^{-3}) in the NCP area, and transported-OOA (33 %) oxidizing from urban emissions. The other two factors include aged hydrocarbon-liked OA (aged-HOA, 28 %) from transported vehicle emissions and biomass burning OA (BBOA, 5 %) from local open burnings. The volatility of total OA (average $C^* = 3.2 \times 10^{-4}$ μg m^{-3}) in this study is generally lower than those in previous field studies, which is mainly due to the high OA oxidation level resulting from aging processes during transport. The volatilities of OA factors follow the order of background-OOA (average $C^* = 2.7 \times 10^{-5}$ μg m^{-3}) < transported-OOA (3.7×10^{-4} μg m^{-3}) < aged-HOA (8.1×10^{-4} μg m^{-3}) < BBOA (0.012 μg m^{-3}), indicating the probable existence of oligomers. The viscosity estimation suggests that the majority of ambient OA in this study behaves as semi-solid (60 %), liquifies at higher RH (21 %), and solidifies (19 %) during noon time when the RH is low and the oxidation level is high. Finally, the estimated mixing time of OA varies dramatically from minutes at night to years in the afternoon, emphasizing the necessity to consider its dynamic kinetic limits when modeling OA. In general, the overall results of this study improve the understanding of the aging impact on OA volatility and viscosity.

1 Introduction

Atmospheric fine particles, which can substantially affect visibility, human health, and climate, have drawn great attention of the public (Song et al., 2018; Quan et al., 2011; Horowitz and Jacob, 1999; Huang et al., 2014; Li et al., 2020b; Huffman et

al., 2009a). In the NCP areas, which is one of the most polluted areas in China, high concentrations of fine particles (21–178 µg m^{-3}) in urban cities have been frequently observed (Zhou et al., 2020; Zhao et al., 2019; Duan et al., 2020; Xu et al., 2019). The city clusters in NCP areas act as urban emission sources and have a great impact on the atmospheric chemistry in the

50   downwind regions. During the transport processes, the pollutants undergo physical and chemical reactions continuously, which significantly change the properties of aerosols, especially for organic aerosols (OA), the dominating component of fine particles (Sun et al., 2017; Zhang et al., 2012; Jimenez et al., 2009; Zhang et al., 2007). In the past decade, plenty of field measurements have been conducted to explore the concentration variations and sources of OA in urban and suburban areas in NCP (Duan et al., 2020; Zhang et al., 2018; Sun et al., 2013; Li et al., 2017a; Hu et al., 2016b; Elser et al., 2016; Hu et al.,

55   2017a; Huang et al., 2010; Jiang et al., 2015; Wang et al., 2015; Xu et al., 2018; Xu et al., 2015; Zhang et al., 2015; Zhang et al., 2016; Zhao et al., 2017; Zhou et al., 2018 and references therein), however, few studies were carried out in background areas (Zhou et al., 2020; Zhang et al., 2020; Zheng et al., 2015; Yan et al., 2021; Du et al., 2015). Studies which focus on the physicochemical properties of OA in background areas, i.e., volatility and viscosity, are even scarce. The volatility and viscosity of OA can determine the gas-particle partitioning and particle phases, which are crucial information to understanding

60   aerosol growth and heterogeneous reactions in bulk OA (Li et al., 2020b; Reid et al., 2018; Shiraiwa et al., 2012). Meanwhile, quantifications of volatility and viscosity of OA in aging plumes are the key information to understand the fate of aerosols in the atmosphere.

Multiple methods have been used to quantify the volatility of OA (Isaacman-Vanwertz and Aumont, 2021; Cappa and Jimenez, 2010; Saha et al., 2015; Li et al., 2016b; Yli-Juuti et al., 2017; Louvaris et al., 2017a). One of the most common methods is

65   combining a heating module (e.g., thermodenuder, TD) with a detection instrument (e.g., aerosol mass spectrometer, AMS) to measure the mass fraction remaining (MFR) of different OA species at various temperatures. The volatility distribution of OA can be estimated based on either an empirical method (Faulhaber et al., 2009) or an evaporation kinetic model (Riipinen et al., 2010; Saha et al., 2015; Cappa, 2010a; Karnezi et al., 2014; Saha et al., 2017; Park et al., 2012; Epstein et al., 2009; Louvaris et al., 2017a). Based on the TD-AMS system, volatilities of ambient OA from urban/suburban (Xu et al., 2021; Louvaris et al.,

70   2017b; Cao et al., 2018; Huffman et al., 2009a; Cappa and Jimenez, 2010; Saha et al., 2018; Paciga et al., 2016; Kang et al., 2022), rural (Zhu et al., 2021) and forest sites (Hu et al., 2016c; Saha et al., 2017; Kostenidou et al., 2018) have been explored. Huffman et al. (2009a) first directly characterized chemically-resolved volatility of ambient aerosols in urban areas, supporting that OA components are semivolatile and POA (primary organic aerosol) is more volatile than SOA (secondary organic aerosol). Using the similar approach, multiple studies (Huffman et al., 2009a; Louvaris et al., 2017b; Xu et al., 2016; Xu et al., 2021;

75   Zhu et al., 2021) found that the OA volatility varies with different emission sources and oxidation levels, usually shows a trend of vehicle OA > biomass burning OA ≈ cooking OA > secondary OA. In addition, extremely low volatility of SOA due to the existence of oligomers after oxidation has also been reported (Lopez-Hilfiker et al., 2016; Hu et al., 2016c). The varied volatilities of POA and SOA emphasize the necessity to investigate OA volatility during aging processes.

Viscosity, which can be influenced by ambient relative humidity (RH), molecular weight, and oxidation level of OA,

80   determines the mixing state and phase state of aerosols (Koop et al., 2011; Shiraiwa et al., 2017; Derieux et al., 2018). Multiple studies in the field campaigns and laboratory experiments suggest that, contrary to the traditional understanding, OA may occur as highly viscous semisolids or amorphous glassy solids under certain conditions (Shiraiwa et al., 2017; Virtanen et al., 2010; Reid et al., 2018; Koop et al., 2011; Renbaum-Wolff et al., 2013), which shows important implications on atmospheric chemistry. Diffusion timescales within aerosols are affected by the aerosol size, mass loading, viscosity, and volatility (Li and

85   Shiraiwa, 2019). The diffusivity of species in aerosol is negatively correlated with viscosity. Thereby it takes a longer time for highly viscous species to reach gas-particle equilibrium, which affects a series of atmospheric processes of aerosols (Shiraiwa and Seinfeld, 2012). By linking with volatility and viscosity based on new parameterization proposed by Li et al. (2020b), the diurnal variations of OA viscosity in ambient air were estimated (Li et al., 2020b; Xu et al., 2021), which can differ more than

4 orders of magnitude between day and night, as well as in the daytime among seasons. The great variation signifies the
90   sensitivity of OA viscosity to ambient conditions.

To investigate OA sources, volatility, and viscosity in the outflow of urban plumes, a TD-AMS system was applied in a ground-based campaign at a continental receptor site of downwind areas in NCP. We systematically investigated the dynamic variations of chemical compositions of fine particles. OA sources were analyzed using Positive matrix factorization (PMF) with Multi-Engine (ME-2) analysis. Coupled with the Hybrid Single-Particle Lagrangian Integrated Trajectory (HYSPLIT) model, the
95   impact of aerosols regional transport was further studied. Finally, a comprehensive understanding of volatilities and viscosities of OA and OA factors during the aging process, as well as their atmospheric implications, are shown and discussed.

2 Experiments

2.1 Field campaign

The field study was conducted at Yellow River Delta National Nature Reserve (YRDNNR) from March 17 to April 12, 2018.
100   The YRDNNR site (37.75° N, 118.97° E, 1 m above sea level) is located in the northeast of Dongying City, Shandong Province, and the estuary of the Yellow River into the Bohai Sea (Yao et al., 2016; Zheng et al., 2019; Zhang et al., 2019), as shown in Fig. 1. Very few industrial or commercial areas were within 15 kilometers of the sampling site, which is considered a regional background site of NCP. The impact of natural oil and gas (NO&G) (i.e. Liquified Petroleum Gas, LPG) and biomass burning on volatile organic compounds (VOCs) and O₃ during the campaign was found (Lee et al., 2021). The wind rose diagram
105   combined with back trajectory clusters in Fig. 1a suggests that the sampling site during this campaign was affected by southern, southeast, and northwest winds, indicating the observed results were strongly influenced by the NCP urban outflows. The average wind speed was 3.0 ± 1.8 m s^{-1} with a range of 0–9.1 m s^{-1}. The average temperature during this study was 11.5 ± 7.0 °C (from −2.8 to 29.2 °C) and RH was 59.1 ± 19.0 % (from 14 to 97 %).
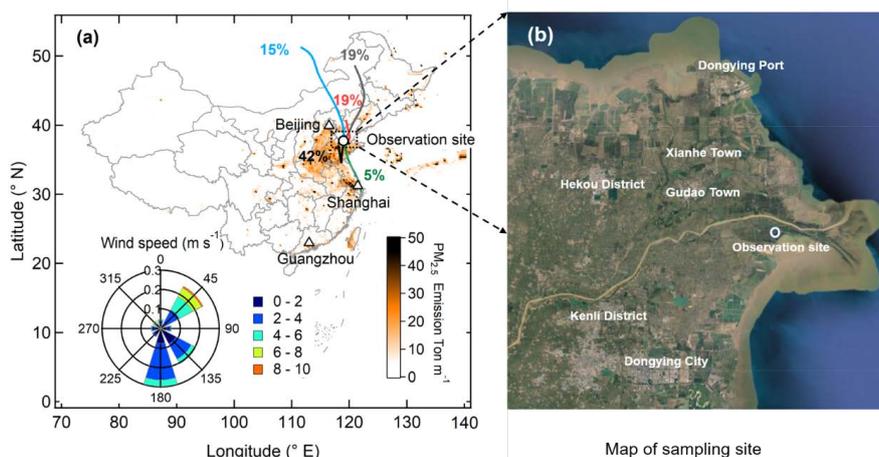
110   **Figure 1. (a) Location of observation site (opaque circle) in the Chinese map, along with wind speeds, wind directions, and back trajectories of air masses during this campaign. The map is color-coded by PM₂.₅ emission inventory (Li et al., 2017b) (b) Map of the Yellow River Delta National Nature Reserve (YRDNNR) region, labeled with the sampling site (opaque circle) and adjacent cities and towns (source: Google Earth).**

2.2 Operations and data processing of instruments

115   ### 2.2.1 HR-ToF-AMS

The chemical composition of PM$_1$ was measured by a high-resolution time-of-flight aerosol mass spectrometer (HR-ToF-AMS, manufactured by Aerodyne Research Inc. ARI, USA; "AMS" will be used hereinafter). The detailed introduction and operating principle of AMS can be found in previously published literature (Canagaratna et al., 2007; Drewnick et al., 2005; Chen et al., 2021b). The setup and calibrations of AMS will be briefly introduced in the following.

120 During this campaign, the ambient air was sampled through a PM$_{2.5}$ cyclone at a flow rate of 5 L min^{-1} and then introduced into AMS through a 1/4-inch stainless steel tube. The sampling flow rate of AMS was 0.1 L min^{-1}. To avoid the effects of varied phase states on the collection efficiency (CE) of particles, a silicon dryer was set ahead of AMS to keep the RH of sampled air below 40 %. The schematic diagram is shown in Fig. S1.

The calibrations including ionization efficiency (IE), inlet flow rate, and sizing distribution were conducted before and after
125 the campaign (Jimenez et al., 2003; Jayne et al., 2000; Canagaratna et al., 2007). The IE calibration was performed based on a brute-force single particle (BFSP) mode (Decarlo et al., 2006), in which 400 nm monodisperse pure ammonium nitrate (NH$_4$NO$_3$) particles were introduced. For mass concentration calculation, the relative ionization efficiency (RIE) of ammonium was determined to be 3.7 by assuming a neutral balance of cation versus anion from standard NH$_4$NO$_3$ signals. And the default RIE values of nitrate, sulfate, chloride, and OA were applied in this study (Huffman et al., 2009a). Taking into account particle
130 loss in AMS, the chemical composition based CE (≈ 0.5) followed by Middlebrook et al. (2012) was applied to correct mass concentration.

Pieber et al. (2016) found that the artificial CO$_2^+$ ion can be caused by inorganic salts due to the interaction between thermal decomposition products of inorganic salts (i.e., NH$_4$NO$_3$) and OA deposit on the vaporizer surface. The ratio of CO$_2^+$/NO$_3^-$ was estimated to be ~ 2.3 % in this study through sampling the pure NH$_4$NO$_3$ particles into AMS. Based on the calibration
135 result, the interference of artificial CO$_2^+$ was excluded in the series of subsequent analyses including OA quantification, elemental ratio calculation, and PMF analysis. Elemental ratios, including oxygen to carbon ratio (O:C), hydrogen to carbon ratio (H:C), and total OA versus organic carbon ratio (OA:OC), were determined by Improved-Ambient (I-A) method in this study (Canagaratna et al., 2015). All the AMS quantification and elemental ratio data used here were based on the "V" mode and analyzed with the software of Squirrel (v1.62G) and PIKA (V. 1.22G) based on Igor pro 6.37.

140 **2.2.2 Other instruments**

The mass concentration of black carbon (BC) was measured by an AE-31 Aethalometer (Magee Scientific, USA) at a time resolution of 5 minutes (PM$_{2.5}$ inlet). A scanning mobility particle sizer (SMPS, TSI, Inc.) was conducted to detect the particle number size distribution (mobility diameter: 15–600 nm) at a time resolution of 5 minutes. The total mass concentration measured by SMPS can be obtained by multiplying the integrated volume concentration (assuming aerosol was spheric) by
145 their corresponding density. The density of the total aerosol (1.63 ± 0.04 g m^{-3} on average) was calculated based on the main chemical components of aerosols measured by AMS and AE-31, as addressed in previous literatures (Decarlo et al., 2008; Hu et al., 2017c; Kuwata et al., 2012). A good agreement of time series between mass concentrations from SMPS and AMS + AE-31 (Slope = 0.97 and R = 0.95, Fig. S2) was found, validating the robust measurement results shown here. Volatile organic compounds (VOCs) were measured by online gas chromatography with a flame ionization detector (GC-FID) at a time
150 resolution of 1 hour (Lee et al., 2021). Regular gases of NO/NO$_2$, SO$_2$, CO, and O$_3$ were measured by NO$_x$ Analyzer (42i), SO$_2$ Analyzer (43i), CO Analyzer (48i), and O$_3$ monitor (49i) from Thermo Fisher Scientific at a time resolution of 1 minute, respectively.

2.3 Source apportionments of PMF and ME-2

Sources of OA components were analyzed based on the conventional positive matrix factorization (PMF) method (Ulbrich et al., 2009) and the multi-linear engine (ME-2) approach (Canonaco et al., 2013). Unconstrained PMF analysis was conducted in PMF Evaluation Tool (PET) v2.08 described in Ulbrich et al. (2009). Compared with conventional PMF, the ME-2 approach allows introducing priori profiles of known OA factors, which can reduce the rotational ambiguity, and directly apportion towards environmentally meaningful solutions (Canonaco et al., 2013). In the ME-2 analysis of this study, we constrained the standard spectrum of BBOA from the Changdao study (Hu et al., 2013) at varied α values using SoFi v6.81. By investigating the characteristics of mass spectra and time series, as well as their correlations with external tracers (Zhang et al., 2014; Ulbrich et al., 2009), four OA factors were finally chosen as the optimum solution for this ambient dataset. The details of PMF and ME-2 analysis can be found in the supporting information (S1.1).

2.4 Thermodenuder and volatility estimation

The TD used in this campaign is a commercial product from ARI and has been applied widely in laboratory experiments (Saha et al., 2015; Huffman et al., 2009b; Grieshop et al., 2009b; Lee et al., 2011; May et al., 2013c; Li et al., 2016a; Saha and Grieshop, 2016; Sato et al., 2018; Champion et al., 2019 and reference therein) and field studies (Huffman et al., 2009a; Hu et al., 2016c; Paciga et al., 2016; Xu et al., 2016; Louvaris et al., 2017b; Cao et al., 2018; Kostenidou et al., 2018; Xu et al., 2021; Zhu et al., 2021 and reference therein). The TD consists of two parts: the heated section and the denuder section. The heated section can realize step-wise heating to obtain concentrations at various temperatures, ranging from 54 ˚C to 230 ˚C in this study. The denuder section was filled with activated charcoal to absorb the gas-phase species evaporated from particles within TD. The setup of the TD-AMS system in this study is shown in Fig. S1, where sampling flow was switched to TD or bypass (ambient) paths at a time resolution of 4 min before being sampled by the AMS and SMPS. The flow rate through the 55 cm heating section was 0.62 L min^{-1}, with a residence time of 20.2 seconds, which is comparable with that (21.2 seconds) used by Huffman et al. (2008; 2009a; b). Bulk particle losses and temperatures in TD were all corrected based on the calibration results from Huffman et al. (2008) since similar TD and its setups in both studies were applied. The corrected centerline temperature is 17 % higher than the measured temperature on average. More detailed information on TD calibrations can be found in S1.2 of the supporting information.

We calculated the MFR of aerosols, which is the ratio of mass concentration through the TD path and bypass path (ambient line) at a set temperature. Then the thermogram, MFR as a function of corrected temperature, can be obtained. The thermograms of each species were depicted to semi-quantitively characterize aerosol volatility (Huffman et al., 2009b). The kinetic limitations of aerosol evaporation exist in TD (Saha et al., 2015), which were mainly influenced by the residence time and OA concentration in TD. Thus it is difficult to directly compare the thermograms in different studies with different residence times and mass loadings (Cain and Pandis, 2017; Karnezi et al., 2014). To further describe the volatility of the complex OA matrix and make it comparable, volatility distribution, expressed as volatility bin set (VBS), was estimated based on the empirical relationship between $LogP_{25}$ and reciprocal of T_{50} developed by Faulhaber et al. (2009). T_{50} represents the temperature value where aerosol species evaporates 50 % compared to the input mass concentration under 25 ˚C (here is referred to as ambient concentration) and P_{25} represents the vapor pressure of species at 298 K. A good agreement of OA volatility between this empirical method and kinetic model method was found previously (Cappa and Jimenez, 2010).

2.5 Predictions of glass transition temperature and viscosity of organic aerosols

Bulk viscosity has been measured directly or indirectly by applying particle rebound, poke flow, and other offline measurements (Liu et al., 2017; Reid et al., 2018; Renbaum-Wolff et al., 2013). Viscosity is associated with the glass transition temperature (T_g), at which the phase transition occurs from semisolid to glassy states (Koop et al., 2011). Recently, more predictive models were developed to estimate the T_g of mixtures in field observations (Shiraiwa et al., 2017; Li et al., 2020b;

Maclean et al., 2021). According to the new parameterization method introduced by Li et al. (2020b), T_g of OA ($T_{g,org}$) at dry
195   conditions was estimated based on OA volatility distribution and the ratio of oxygen to carbon (O:C, "Aiken-Ambient" method).
The T_g of OA–water mixtures ($T_{g,oorg}$) at a given RH can be estimated using the Gordon–Taylor equation, in which the aerosol
water content associated with OA can be calculated by the effective hygroscopicity parameter (κ) (Mei et al., 2013; Mikhailov
et al., 2009). Finally, viscosity can then be calculated by applying the modified Vogel–Tammann–Fulcher (VTF) equation
(Angell, 1991; Derieux et al., 2018). τ_{mix}, representing the timescale that reaches diffusion equilibrium in bulk particles, can
200   be estimated by the equation: $\tau_{mix} = d_p^2/(4\pi^2 D_b)$ (Seinfeld and Pandis, 2016), where d_p is the particle diameter (assuming 200
nm), and the bulk diffusion coefficient D_b is calculated from the predicted viscosity by the fractional Stokes-Einstein relation
(Xu et al., 2021; Evoy et al., 2019). The detailed computational processes can be found in S1.3 of the supporting information.

2.6 Air mass trajectory analysis

Back trajectories analysis with altitude at 100 m were calculated every 6 h during this campaign using the HYSPLIT model
205   (http://ready.arl.noaa.gov/HYSPLIT.php) developed by the Air Resources Laboratory (ARL) of the National Oceanic and
Atmospheric Administration (NOAA) (Draxier and Hess, 1998; Cohen et al., 2015). The weather data were obtained from the
Global   Data   Assimilation   System   (GDAS)   archived   by   NOAA   Air   Resources   Laboratory
(ftp://arlftp.arlhq.noaa.gov/pub/archives/). Then the back trajectories were divided into several groups based on their similarity
in spatial distribution (cluster analysis) (Zheng et al., 2010).

210   In addition, the potential source contribution function (PSCF) (Polissar et al., 1999; Zhang et al., 2013) was also applied here
to investigate the contribution of regional transport. This analysis was achieved through the "Zefir" software, which is an Igor-
based package and specifically designed to achieve a comprehensive geographical origin analysis using a single statistical tool
(Petit et al., 2017). Pollutant concentrations were put into "Zefir" software together with data obtained from HYSPLIT and
NOAA. The geographic region was divided into 0.5×0.5° grid cells (latitude i and longitude j). If the endpoint of the trajectory
215   falls into a grid cell, the total number of trajectories is calculated as n_{ij}, and the number of these endpoints which are higher
than a threshold (75th percentile used here) is counted as m_{ij} (Liu et al., 2021). To reduce the bias of PSCF for grid cells with
low values of n_{ij}, the weight function (w_{ij}) recommended by Waked et al. (2014) was applied to the PSCF.

$$W_{ij} = 1\,, for\ n_{ij} > 0.8 * \max(log_{(n+1)})$$

$$0.725, for < 0.6 \max(log_{(n+1)}) * n_{ij} \le 0.8 * \max(log_{(n+1)})$$

220    $$0.35, for < 0.35 \max(log_{(n+1)}) * n_{ij} \le 0.6 * \max(log_{(n+1)})$$

$$0.1\,, n_{ij} \le 0.35 * \max(log_{(n+1)})$$

3 Results and discussion

3.1 Concentrations of PM$_1$ chemical compositions

The time series of mass concentration from the main components in PM$_1$ are shown in Fig. 2. The overall PM$_1$ concentration
225   ranged dramatically from 2.5 to 152.8 μg m^{-3} with an average value of 31.5 ± 22.7 μg m^{-3} (Fig. 2a, Table 1), which is generally
lower than the average values in urban areas of NCP, e.g., 45 – 53 μg m^{-3} in the spring of Beijing (Hu et al., 2017a; Sun et al.,
2015). During this campaign, nitrate was the dominant species, accounting for 33 % of total PM$_1$ mass concentration, then
followed by OA (25 %), sulfate (17 %), ammonium (17 %), BC (4 %), and chloride (3 %) (Fig. 2b).

When the mass concentration of PM_1 is below 20 μg m^{-3} (Fig. 2c), OA and sulfate account for the largest proportion, about
230 40 % and 22 % respectively. Nitrate increases dramatically and reaches 39 % of PM_1 in the polluted periods (tinted by yellow
color in Fig. 2a). The NO_2^+/NO^+ ratio of ambient nitrate in AMS (average value = 0.27) is similar to the ratio from pure
ammonium nitrate calibration (average value = 0.28) (Fig. S7), suggesting that the observed nitrate here is nearly inorganic (>
90 %). An increase in inorganic nitrate at higher aerosol concentration has also been observed in other field studies including
urban areas (Chen et al., 2021a; Chen et al., 2021b; Griffith et al., 2015; Li et al., 2018), downwind sites (Qin et al., 2017; Li
235 et al., 2020a) and also other receptor sites (Hu et al., 2013; Li et al., 2014). As the air quality control policy was continuously
performed in China, the emission of SO_2 decreased substantially compared to that of NO_2, and nitrate becomes the dominant
secondary component in the fine particles (Xie et al., 2020; Geng et al., 2017a; Li et al., 2019).

The formation of nitrate has been identified as the following two main chemical pathways: (1) homogeneous reaction of
gaseous nitric acid (HNO_3) and ammonia (NH_3), in which HNO_3 is largely produced by photochemical oxidation of NO_2 by
240 OH radicals in the daytime (Yang et al., 2022); (2) Heterogeneous hydrolysis of dinitrogen-pentoxide (N_2O_5), which is the
major source of HNO_3 at night (Griffith et al., 2015); In general, abundant precursors, high pH and aerosol liquid water content
(ALWC) during polluted periods might further promote these two processes (Chen et al., 2021b; Wang et al., 2020). In the
remote receptor site of this study, in addition to the chemistry process, regional transport is another important source of high
nitrate mass concentration (Squizzato et al., 2012). In this study, increased nitrate was observed when the southeast to
245 southwest winds dominated with the continuously high-speed wind (above 8 km h^{-1}) (Fig. 3a1), suggesting that regional
transport in winter and spring of NCP areas played an important role in the enhanced nitrate observed here (Huang et al., 2020;
Hu et al., 2016b). The sulfate, ammonium, and BC show similar patterns as nitrate in diurnal variations (Fig. 2d) and bivariate
polar plots (Fig. 3), supporting the upwind anthropogenic emissions were transported to the regional receptor areas in the
downwind direction. The PSCF results based on backward trajectory analysis were applied to further explore the potential
250 transport from different regions to this receptor site. High concentrations of secondary inorganic aerosols were mainly
contributed by the west and south regions of Shandong province, and the northern part of Anhui and Jiangsu province, where
high anthropogenic $PM_{2.5}$ emissions exist (Lei et al., 2011; Geng et al., 2017b). The results again suggest the important transport
influences on aerosol chemistry from NCP urban outflows to receptor areas.

Table1. Summary of average mass concentrations of PM_1 species and OA components (μg m^{-3}), average mixing ratios
255 **of gas-phase pollutants, and values of meteorological parameters during the entire campaign and polluted period. The**
polluted period definition can be found in the caption of Fig. 1.

	Dongying Spring (Average± SD)	
	Entire Study	Polluted Period
Total PM_1 (μg m^{-3})	31.5 ± 22.7	50.3 ± 5.4
Total OA (μg m^{-3})	7.9 ± 4.5	12.5 ± 4.1
BBOA	0.4 ± 0.7	0.7 ± 0.7
HOA	2.2 ± 2.0	3.5 ± 2.6
Transported-OOA	2.6 ± 2.7	5.1 ± 2.8
Background-OOA	2.6 ± 1.6	3.1 ± 1.7
Sulfate (μg m^{-3})	5.3 ± 3.9	8.0 ± 3.7
Total Nitrate (μg m^{-3})	10.6 ± 9.4	17.4 ± 8.5
Inorganic nitrate	10.0 ± 9.3	16.8 ± 8.7
Organic nitrate	0.9 ± 0.8	0.7 ± 0.9
Ammonium (μg m^{-3})	5.5 ± 4.4	8.9 ± 4.0

Chloride (µg m⁻³)	1.0 ± 1.6	1.7 ± 2.0
BC (µg m⁻³)	1.2 ± 0.8	1.8 ± 0.7
NH_3 (ppb)	26.7 ± 19.0	15.6 ± 11.6
CO (ppm)	0.5 ± 0.3	0.6 ± 0.3
NO (ppb)	0.9 ± 2.1	1.3 ± 2.5
NO_2 (ppb)	11.8 ± 7.2	16.5 ± 6.8
SO_2 (ppb)	3.1 ± 3.5	4.9 ± 3.8
O_3 (ppb)	47.1 ± 22.2	51.4 ± 25.5
Wind speed (m s⁻¹)	3.1 ± 1.8	2.6 ± 1.4
Temperature (℃)	10.5 ± 7.2	15.6 ± 6.0
RH (%)	60.7 ± 19.2	57.9 ± 18.1
ALWC (µg m⁻³)	13.3 ± 18.3	23.6 ± 63.0
pH	3.9 ± 0.7	3.7 ± 0.7
Pressure (hPa)	101.4 ± 0.7	101.1 ± 0.4

Total PM_1 = OA + Sulfate + Nitrate + Ammonium + Chloride + BC
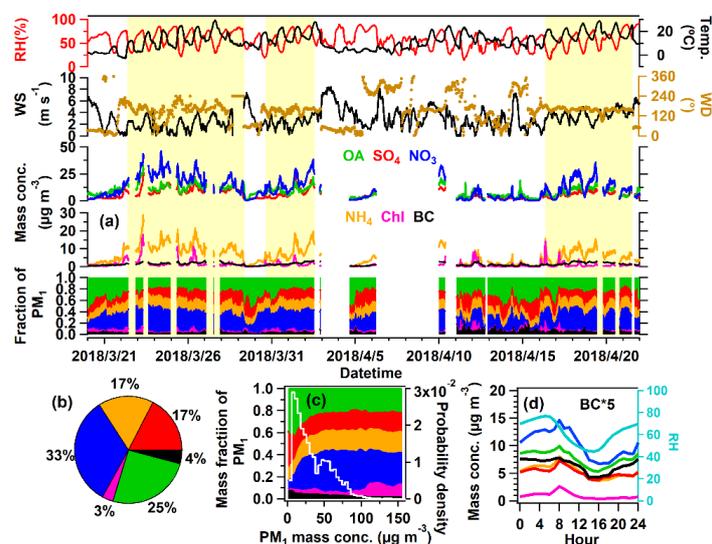
Figure 2. (a) Time series of main species in PM_1 and meteorological parameters (relative humidity, temperature, wind speed, and
260   wind direction). The yellow background represents the polluted period in this campaign, which was selected based on mass
concentration of total PM_1 above 20 µg m⁻³ and lasts for at least 2 days, accompanied by continuous south winds; **(b)** Average
chemical compositions of PM_1; **(c)** Variations of main compositions (left axis) and probability density as a function of PM_1 mass
concentration (right axis); **(d)** Average diurnal variations of PM_1 species and PBL height during the entire campaign.
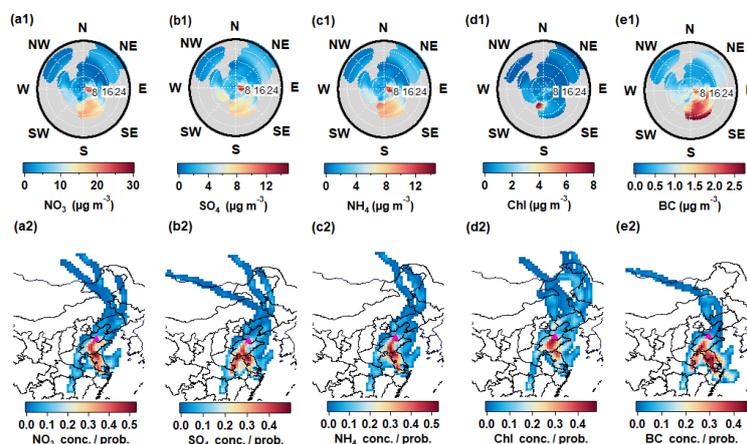
Figure 3. Bivariate polar plots and the results of potential source contribution function (PSCF) from inorganic species, including (a1, a2) NO_3; (b1, b2) SO_4; (c1, c2) NH_4; (d1, d2) Chl; (e1, e2) BC. The unit of wind speed is km h^{-1}.

3.2 Source apportionment of OA

Four OA factors were resolved in this study, including BBOA (5 %), aged-HOA (28 %), transported-OOA (33 %), and background-OOA (33 %) respectively, as shown in Fig. 4.

3.2.1 Biomass Burning OA (BBOA)

BBOA in this study was possibly from (1) biofuel/biomass burning from domestic heating in the NCP (Duan et al., 2020; Huang et al., 2020; Elser et al., 2016); (2) The open biomass burning around observation site (Li et al., 2017a; Liang et al., 2021). It is indeed that biomass burning plumes from open fire burning were frequently seen during the campaign. As shown in Fig. S8, a positive correlation between BBOA with surrounding fire counts was found, suggesting that open biomass burning might play a more important role than domestic heating. Potassium (K^+), regarded as a good indicator of biomass burning (Aiken et al., 2010) also showed a good correlation with BBOA (R = 0.6), validating the BBOA resolved here.

$C_2H_4O_2^+$ ion, which is mainly produced by the oxidation process of anhydrous sugars (pyrolysis products of cellulose and lignin such as mannose and levoglucosan) (Bertrand et al., 2018), was found to be a tracer for BBOA (Cubison et al., 2011). As depicted in Fig. S9a, the higher f_{60} value in OA above the background level (0.3 %) is concurrent with an increased BBOA fraction. The O:C value of BBOA is 0.37, which is in the range of reported values (0.2–0.65) from primary BBOA observed in other studies (Zhou et al., 2020; Hu et al., 2016b; Xu et al., 2017; Zhang et al., 2016). According to the bivariate polar plot and PSCF result of BBOA in Fig. 5b, the higher concentration of BBOA partially comes from local emission of biomass burning southeast of the sampling site.

3.2.2 Aged hydrocarbon-like OA (aged-HOA)

HOA has been widely recognized and elaborated on in previous studies (Hao et al., 2014; Hu et al., 2016b; Aiken et al., 2009; Huang et al., 2020; Sun et al., 2014; Zhang et al., 2011; Zhou et al., 2020; Zhang et al., 2005a; Zhang et al., 2007; Ng et al., 2011b). The HOA resolved in this study is not only contributed by fragments of C_xH_y (C_nH_{2n+1} and C_nH_{2n-1}, m/z 55, 57, 69, 81, 91, etc.) which is similar to the reported reference spectra of HOA (Hu et al., 2013; He et al., 2011; Ng et al., 2011a; Zhang et al., 2005b; Zhu et al., 2021; Jimenez et al., 2009) but also includes a high abundance of oxygenated ions (i.e., CO_2^+). It suggests that the HOA resolved here is partially aged, and thus is entitled to aged-HOA. The diurnal variations of aged-HOA mass concentration and its fraction in total OA, show a prominent peak during the traffic rush in the morning (8:00 am), then decrease

sharply with the elevated boundary layer, suggesting this factor is mainly influenced by primary emissions (Fig. 4, Fig. S10). The primary property of aged-HOA in this study was also identified by their good correlation with primary anthropogenic VOCs of benzene and ethyl toluene (with R = 0.82 and 0.8 respectively) (Hu et al., 2016a; Lee et al., 2015; Mohr et al., 2012).

295 The average O:C value of aged-HOA in this campaign is 0.55, which is out of the range of O:C of HOA observed in China (0.05–0.44) (Hu et al., 2013; Zhou et al., 2020; Hu et al., 2016c). The high O:C value of aged-HOA in this study was probably due to the long-distance transport from surrounding urban/town areas (Fig. 1a). Based on the bivariate polar plot and PCSF analysis in Fig. 5c, the higher aged-HOA concentration was in accord with urban plumes originating from the west to south region, where a nearby Dongying city is also on this path.

3.2.3 Transported-OOA and Background-OOA

Transported-OOA and background-OOA, representing two types of SOA with different origins, were resolved in this study. Both factors are fairly oxidized, which are characterized by the high mass abundance of oxidized m/z 44 and m/z 28 in total OA (0.23 for transported-OOA, 0.21 for background-OOA). Transported-OOA has an O:C ratio of 0.97, which is slightly lower than the 1.1 for background-OOA. Both OOA factors are in the high range compared with most OOA factors observed

305 in urban and suburban areas (0.29–1.3) (Li et al., 2015; Xu et al., 2019) and remote areas (0.47–1.45) (Zhou et al., 2020; Zheng et al., 2017; Gong et al., 2012).

The transported-OOA shows good correlations with secondary inorganic sulfate and nitrate (R = 0.81 and 0.83 shown in Fig. S5, respectively), consistent with its secondary origins of OOA (He et al., 2011; Huang et al., 2020; Zhang et al., 2005a). The regression ratio between transported-OOA vs. sulfate + nitrate is around 0.84, within the range obtained in NCP areas (0.51–

310 0.93) (Sun et al., 2016; Sun et al., 2012; Huang et al., 2010). Similar to the sources of secondary inorganic aerosols, the higher transported-OOA concentration might correspond to the transport process from urban emissions located in the southern region of the sampling site, as shown in the bivariate polar plots and PSCF results (Fig. 5d). The background-OOA has a relative flat diurnal variation (Fig. 4g) and shows enhanced mass concentrations in all directions in the bivariate polar plot (Fig. 5e1), consistent with its background origins and representing the background concentration in NCP (2.6 ± 1.6 µg m^{-3}).

315 On average, the sum of transported-OOA and background-OOA can account for 66 % of total OA. When the total OA concentration is below 3 µg m^{-3}, background-OOA accounts for nearly 50 % of the OA mass concentration as shown in Fig. 4f. While the total OA increases from 4 to 20 µg m^{-3}, the transported OOA from urban plumes starts to dominate (from 20 % to 44 %). The dominance of OOA contribution to OA is consistent with findings in the urban outflow of Mexico City (Jimenez et al., 2009). As OA concentration enhances above 20 µg m^{-3}, the aged-HOA and BBOA fractions increase from 29 % to 53 %

320 and 6 % to 16 %, respectively, confirming the primary anthropogenic emission is still an important contributor to the air pollution periods at a remote receptor site.

10.5194/acp-2022-575
2022-08-26
Atmospheric Chemistry and Physics
en
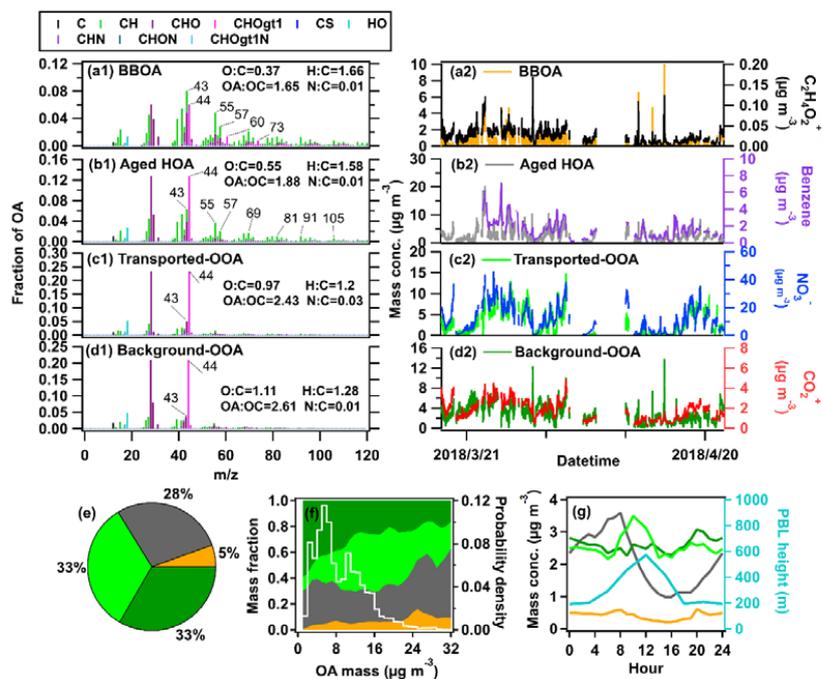
Figure 4. Mass spectra (left) and time series (right) of four OA factors: (a1, a2) BBOA, (b1, b2) aged-HOA, (c1, c2) transported-OOA, (d1, d2) background-OOA; Time series of tracers associated with each factor were also displayed. (e) Average chemical compositions of OA; (f) Variations of OA compositions as well as probability density as a function of OA mass concentration. (g) Average diurnal variations of OA factors and planetary boundary layer (PBL) height during the whole campaign.
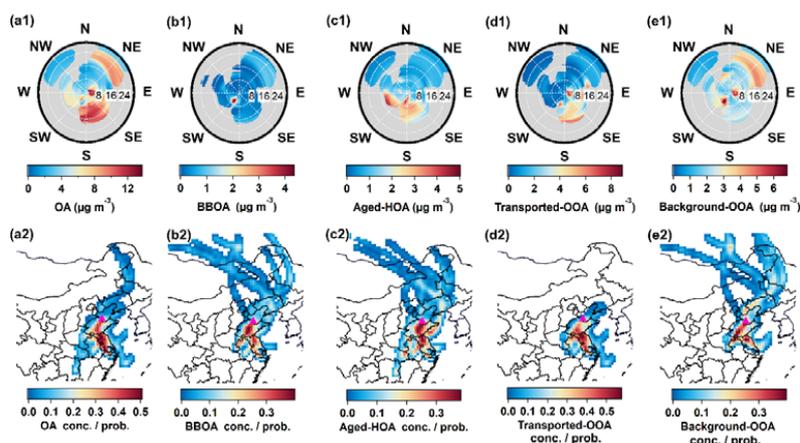
Figure 5. Bivariate polar plots and PSCF results of organic components, including (a1, a2) total OA; (b1, b2) BBOA; (c1, c2) Aged HOA; (d1, d2) transported-OOA; (e1, e2) background-OOA. The unit of wind speed is km h⁻¹.

3.4 Volatility of PM₁ species and OA factors

3.4.1 Volatility of inorganic species

Fig. 6 shows the thermograms of non-refractory aerosols as well as their main chemical components. As the TD temperature increases, the MFR of sulfate keeps constant until 115 °C, leading to a slight increase in its fraction in total PM₁. The less steep thermogram of sulfate than those of other species is mainly due to the low volatility and its slight increase of collect efficiency

335   caused by phase variation upon heating (Huffman et al., 2009a), which have been consistently observed in laboratory
experiments (An et al., 2007; Huffman et al., 2009a) and field studies (Cao et al., 2018; Huffman et al., 2009a; Xu et al., 2016;
Xu et al., 2021; Kang et al., 2022). When TD temperature is above 150 °C, the MFR curve of sulfate descends sharply to 6.5 %.
However, higher residual of sulfate in this study compared to that of pure $(NH_4)_2SO_4$ from our laboratory experiment indicates
that partial sulfate signals detected by AMS might be organic sulfates or metallic sulfates (Fig. 6c). The decreased $H_2SO_4^+/SO_4^+$,

340   HSO_3^+/SO_4^+, SO_3^+/SO_4^+ ratio and increased SO_2^+/SO_4^+ ratio as functions of TD temperature indeed were observed (Fig. S11),
indicating the possible existence of organic sulfate (Chen et al., 2019). The $CH_3SO_2^+$ ion (m/z 78.99), which was considered
to be a fragment ion from methanesulfonic acid (MSA) influenced by marine aerosols (Zhou et al., 2016; Huang et al., 2015;
Zorn et al., 2008) and also possibly an indicator of sulfur-containing aerosols influenced by traffic and fossil carbon in urban
areas (Daellenbach et al., 2017; Vlachou et al., 2019), shows higher volatility than sulfate in this study. The higher volatility

345   of the $CH_3SO_2^+$ ion is probably because of its different bond types connected to the sulfate group than sulfate (Chen et al.,
2019). Similar higher volatility of laboratory generated-MSA particles than that of ammonium sulfate is also observed in this
study (Fig. 6c), which is consistent with the ambient results.

To quantitively compare the thermograms of different species, T_{50}, the temperature when MFR is equal to 0.5 is used here
(Faulhaber et al., 2009; Cappa, 2010b). To obtain the T_{50} more accurately, the thermograms were fitted by Hill's Equation

350   (S1.2 in supporting information) (Emanuelsson et al., 2013; Kolesar et al., 2015). Compared to sulfate (T_{50} = 159 °C), the T_{50}
values of nitrate and chloride are 57 °C and 61 °C (Figs. 6d and e), respectively, supporting their semi-volatile properties in the
ambient air (Cao et al., 2018; Xu et al., 2016; Xu et al., 2021). The evaporated loss of ambient nitrate has also been frequently
observed in the offline membrane samples, in which 60–80 % of nitrate can evaporate in the summer (Chow et al., 2005;
Hering and Cass, 1999). The similar phenomenon of NH_4NO_3 evaporation (30–40 %) has been found in the field-deployed

355   oxidation flow tube, the temperature inside of the reactor is about 10 °C higher than that in the ambient air due to the heated
cabinet of the airplane (Nault et al. 2018). Despite the quick evaporations of ambient nitrate and chloride, their T_{50} values are
still higher than those of pure ammonium salts (i.e., NH_4NO_3 and NH_4Cl) generated by an atomizer in the laboratory
experiments (T_{50} = 37 °C and 54 °C, respectively). When TD temperature is above 150 °C, compared to the complete
evaporations of pure NH_4NO_3 and NH_4Cl (Fig. 6), ~ 5 % of nitrate and ~ 10 % of chloride in ambient air remained. The

360   fractions of nitrate and chloride in total PM_1 species also increase from 5 % and 1 % at middle temperatures to 14 % and 3 %
at higher temperatures (> 180 °C). These increases have also been observed in other field studies conducted with the TD-AMS
system (Huffman et al., 2009a; Xu et al., 2019). For nitrate, the high remaining fraction is probably caused by the partial
contribution from organic nitrate or non-refractory inorganic salts (e.g., $NaNO_3$). This deduction is supported by the
continuously decreased NO_2^+/NO^+ ratio (0.06 finally), consistent with similar low values in organic nitrate ($\approx$ 0.1, a factor of

365   2.75 lower than the ratio of 0.28 in NH_4NO_3) (Day et al., 2022; Fry et al., 2013) and $NaNO_3$ ($\approx$ 0.006, a factor of 50 lower)
(Hu et al., 2017c). The mass remaining fraction of chloride might indicate the presence of metallic chlorides, such as $ZnCl_2$,
$PbCl_2$, and KCl, which are usually emitted from combustion sources at high temperatures (Huffman et al., 2008; Xu et al.,
2019; Aiken et al., 2009; Moffet et al., 2008).

Quick evaporation of ammonium species than cation species during heating was observed, leading to acidified aerosols

370   (measured NH_4/predicted NH_4 < 1) (Fig. 6f). This is mainly due to the decomposition of ammonium salts and yield of gas-
phase NH_3 upon heating (Hu et al., 2017b). Similar behavior of acidified aerosol in the TD line was exhibited in other field
studies (Huffman et al., 2009a; Denkenberger et al., 2007).

In summary, the volatility of inorganic species ranked in the sequence of nitrate > chloride > ammonia > sulfate in this study.
Compared to their pure ammonium salts, all ambient inorganic aerosols had lower volatilities and part of them remained at

4000

high temperatures, indicating the existence of low volatile metallic or organic-related species in AMS detected signals. These results support the complex property of ambient aerosols.
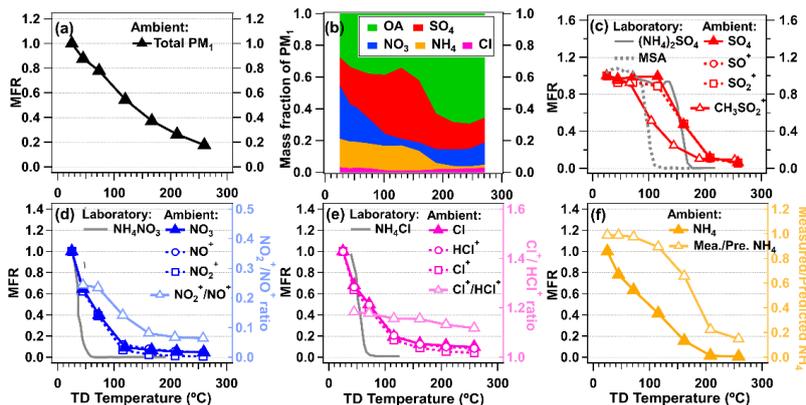
Figure 6. (a) Mass fraction remaining (MFR) of total NR-PM₁; (b) Fraction of main components in NR-PM₁ as a function of TD temperature; (c) Variations in the average MFR of the inorganic species with their corresponding constituent ions as functions of TD temperature: (c) sulfate; (d) nitrate; (e) chloride; (f) ammonium. In addition, MFRs of pure ammonium salts of sulfate, nitrate, and chloride, as well as methanesulfonic acid (MSA) measured in this study were shown for comparison. Particle acidity calculated as the measured NH₄ vs predicated NH₄ assuming a neutral balance from aforementioned cations as a function of TD temperature is also shown in the right axis of panel (f).

3.4.2 Volatility of OA and different OA factors

The thermograms of total OA and OA factors are shown in Fig. 7. The T_{50} of total OA is about 105 °C, which is higher than that of nitrate (T_{50} = 57 °C), while lower than that of sulfate (T_{50} = 159 °C). Total OA thermograms in Riverside, LA and Mexico City are also shown in Fig. 7a. Thermograms of these three studies should be comparable since they have a similar residence time of TD (about 21s) and OA concentration (7.9–19.9 µg m⁻³ in average) (Huffman et al., 2009a; Docherty et al., 2011; Aiken et al., 2009), as well as the similar TD setup. During these two campaigns in Riverside, LA and Mexico City, the T_{50} of OA (92 °C and 86 °C respectively) are lower than that obtained in Dongying (T_{50} = 105 °C). The slightly lower volatility of OA in Dongying is reasonable since the OA is more oxidized (O:C = 0.85) than those from Riverside, LA and Mexico City (O:C = 0.45 and 0.54 respectively) (Aiken et al., 2008; Docherty et al., 2011).

To further compare the volatility results among more studies, the volatility distribution of OA was estimated based on the empirical method of Faulhaber et al. (2009). As is shown in Fig. 8a, the volatility of OA was distributed in the range of C* = 10⁻⁹–10² µg m⁻³ with two prominent peaks around C* = 10² and 10⁻⁴–10⁻³µg m⁻³. If we categorize the entire distribution into different groups based on volatility introduced by Seinfeld and Pandis (2016), the OA in this study is composed of 52 % extremely low volatile organic compounds (ELVOCs, C* ⩽ 10⁻⁴ µg m⁻³), 26 % low volatile organic compounds (LVOCs, 10⁻⁴ < C* ⩽ 10⁻¹ µg m⁻³) and 22 % semi-volatile organic compound (SVOCs, 10⁻¹ < C* ⩽ 10² µg m⁻³). The SVOC fraction in this study is lower than the values from urban areas (37–67 %), however, is higher than that of OA strongly influenced by biogenic emissions (11–16 %), as shown in Fig. 9a. The former is mainly due to the OA in this study being more oxidized than those from urban areas where fresh primary emissions impact strongly. The lower SVOC fraction of OA in forest areas is reasonable since the OA is mainly composed of the high fraction of biogenic SOA, which is strongly influenced by isoprene and monoterpene emissions. The autoxidation and oligomerization during biogenic SOA formation leading to lower volatility have also been reported (Ehn et al., 2014; Bianchi et al., 2017; Lopez-Hilfiker et al., 2019).

405   To further investigate the OA volatilities from different sources, the fractions of OA factors as a function of TD temperature
and their thermograms are shown in Figs. 7b–f. In general, aged-HOA, whose MFR is also characterized by its internal tracers
($C_xH_y^+$), is the most volatile component before 120 ℃ among all OA factors. During this campaign, half of aged-HOA
evaporates at ~ 77 ℃ (T_{50}), which is similar to those in Mexico City (T_{50} = 68 ℃) and Riverside, LA (T_{50} = 82 ℃). While the
temperature is above 100 ℃, the MFR of aged-HOA in this study is much higher than those in the other two campaigns

410   (Huffman et al., 2009a), consistent with that HOA was oxidized during the transport process leading to a lower volatility. As
shown in the plots of volatility distributions in Figs. 8b and 9b, the non-volatile ELVOC and LVOC fraction of aged-HOA is
around 60 % in this study, which is higher than the HOA obtained in other areas (21–40 %), however, similar to the HOA value
obtained in Athens during wintertime (72 %, Fig. 9b), which was also conducted at an urban background site. This suggests
the aging processes greatly decrease the POA volatility. For the laboratory-generated POA from diesel/gasoline emissions,

415   their non-volatile fractions only account for 3–27 % of OA, indicating much higher volatility of POA than that of ambient
HOA. The lower volatility supports that ambient HOA resolved in ambient air is a complex mixture and might be partially
oxidized (Cappa and Jimenez, 2010). We examined if low volatile PAH compounds might contribute to the low volatility of
HOA, whereas negligible PAH ions contribution to OA was found. This suggests the PAH is not the main reason leading to
the high non-volatile contribution of aged-HOA.

420   The thermogram of BBOA is shown in Fig. 7d. The T_{50} of BBOA in this study is 81 ℃, which is comparable with the T_{50} of
HOA (77 ℃) in this study. However, the BBOA shows a much lower residual (< 5 %) than that of HOA when TD temperature
is above 150 ℃, consistent with the fact that BBOA observed here is fresher and more local than aged-HOA. Although BBOA
is the most volatile factor resolved in this study, it still shows the highest non-volatile fraction (72 %) compared with the results
of BBOA in other studies (31–49 %) (Fig. 9c). The diversity of BBOA volatility distributions might be caused by the different

425   burning materials and conditions, as well as the influence of aging processes (Huffman et al., 2009b; May et al., 2013c; Xu et
al., 2021). It is also supported by the fact that ambient BBOA show lower volatility than that of laboratory-generated BBOA
from different combustion conditions (Grieshop et al., 2009a; Grieshop et al., 2009b; May et al., 2013c), emphasizing the
aging impact on ambient BBOA volatility.

The thermograms of transported-OOA and background-OOA are shown in Figs. 7e and f. Obvious lower volatility of

430   background-OOA than that of transported-OOA was found, which is consistent with the slightly higher O:C value of the latter
(1:1 vs 0.97). The thermogram of the CO_2^+ ion, a reliable signature of SOA from thermal decarboxylation of organic acids in
AMS (Aiken et al., 2009; Ng et al., 2010), more resembled the thermogram of background-OOA, consistent with the finding
that highly oxidized OA is mainly composed of organic acids (Chen et al., 2020). We compared the volatilities of the two OOA
factors resolved in this study to those reported in other ambient campaigns in Fig. 9d. It was found that the non-volatile fractions

435   of transported-OOA and background-OOA (both are 82 %) are only lower than that from LV-OOA obtained in Mexico City
(98 %) (Cappa and Jimenez, 2010), however, are higher than those from the majority of other urban OOA factors (27–71 %).
This is consistent with the fact that in addition to POA the aging process can substantially decrease the SOA volatility in
ambient air as well. Meanwhile, we found the SOA volatility in this study is comparable to that of isoprene-expoxydiol derived
SOA (IEPOX-SOA, ELVOC+LVOC = 87–98 %), a large fraction of which was composed of oligomers (Hu et al., 2016c;

440   Krechmer et al., 2015), suggesting the probable existence of oligomers in the two very aged SOA resolved here.

By summarizing all the average volatilities of OA and OA factors in previous and this studies (average log C* ranged from –
5.34 µg m^{-3} to –0.015 µg m^{-3}), the scatter plot of O:C vs average log C* is shown in Fig. 10. In general, the average log C*
exhibits slight dependence on the ratio of O:C (slope = –0.18), which do not show a clear trend as found in the laboratory SOA
(Jimenez et al., 2009). The difference is possibly due to that oligomerization and decomposition might result in different

445   volatilities, however, with similar O:C values (Hildebrandt et al., 2010; Kroll and Seinfeld, 2008). E.g., previous studies have

shown that the OA, oligomers, in particular, can decompose to more volatile components or form new/less non-volatile species upon heating (Cappa and Jimenez, 2010). Thus, the fraction of oligomers in OA did not show the same trend with O:C ratios during the heating process (Zhao et al., 2020). In addition, the ambient RH made the relationship between OA volatility and its O:C more complicated. On the one hand, the aqueous-phase reaction has been supposed to be an important pathway for the

450   formation of low volatility and higher molecular weight compounds (e.g., oligomer) (Zhou et al., 2016). While on the other hand, the volatility of OA increases after hydrolysis (Emanuelsson et al., 2013; Claflin and Ziemann, 2019). Therefore, the results here suggest that the ambient O:C ratio may not be a robust indicator of OA volatility among different studies based on heating detection techniques (Huffman et al., 2009a; Denkenberger et al., 2007; Cerully et al., 2015; Zhao et al., 2020).

Further, we investigated the evaporation loss of OA due to dilution, which is mainly dependent upon its non-volatile/volatile

455   fraction. The higher amounts of non-volatile species exist, the lower evaporation losses to OA dilution. Finally, the evaporation loss of dilution followed reversely the order of the fraction of non-volatile species (f_{nv}), aged-HOA (f_{nv} = 0.63) > BBOA (f_{nv} = 0.72) > transported-OOA (f_{nv} = 0.82) ≈ background-OOA (f_{nv} = 0.82), as shown in Fig. 8f. After a factor of 10 dilution, aged-HOA would evaporate 30 % at ambient temperature, which suggests that even the HOA is pretty aged in this study and it can still be oxidized continuously, thus contributes the SOA formation during the long-distance transport. This suggests a high

460   SOA formation potential in the outflow of NCP urban emissions.
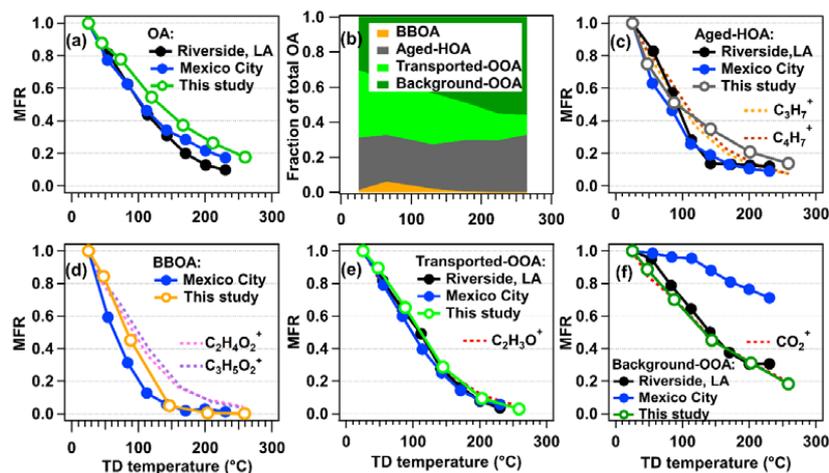
Figure 7. (a) Thermogram of total OA; **(b)** Fraction of four factors in total OA as functions of TD temperature; MFRs of **(c)** aged-HOA, **(d)** BBOA, **(e)** transported-OOA, and **(f)** background-OOA. For comparison, the MFR curve observed in other campaigns, such as Riverside, Los Angeles, USA, and Mexico City, Mexico (Huffman et al., 2009a) are also shown together due to their similar

465   residence time in TD, which are marked by black and blue solid circles, respectively.
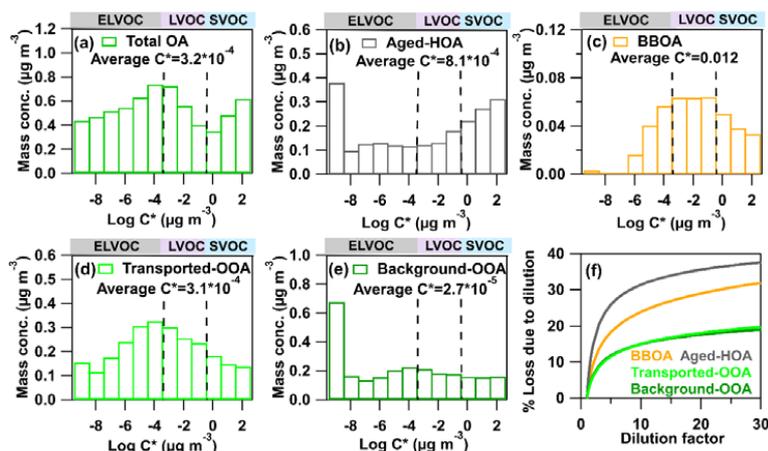
Figure 8. Volatility distributions of (a) total OA, (b) aged-HOA, (c) BBOA, (d) transported-OOA, (e) background-OOA. The unit of average C* is µg m^{-3}. (f) The additional mass losses (E$_{loss}$) of four OA factors as functions of the dilution factor.
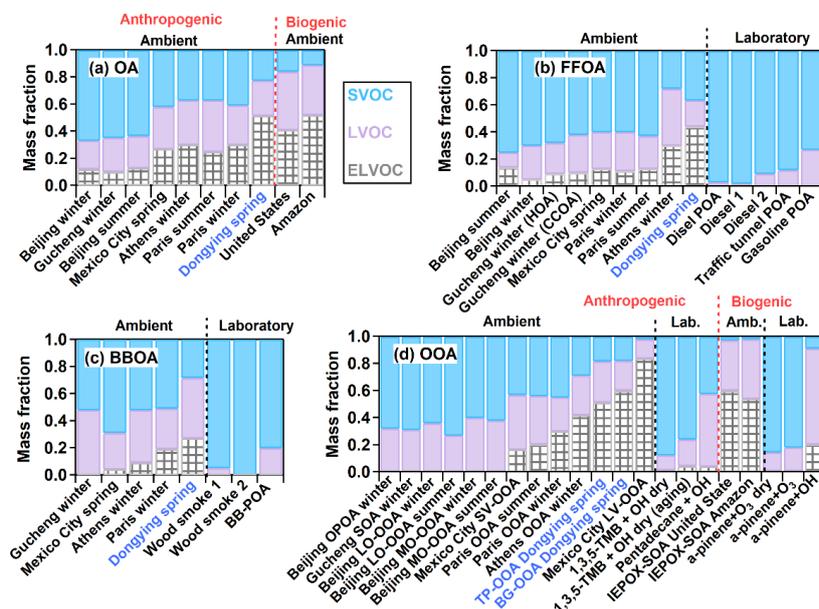
Figure 9. Fractional contributions of various types of OA for different studies, including studies in Dongying (this study), Beijing and Gucheng (Xu et al., 2021), Paris (Paciga et al., 2016), Athens (Louvaris et al., 2017b), Mexico City (Cappa and Jimenez, 2010), southeastern of United State and Amazon (Hu et al., 2016c) and several laboratory experiments (Grieshop et al., 2009b; Grieshop et al., 2009c; Li et al., 2016a; May et al., 2013a; May et al., 2013b; May et al., 2013c; Sato et al., 2018; Sato et al., 2019; Ylisirniö et al., 2020). Detailed data can be found in Table S2–S5. In panel (b), FFOA (fossil fuel-related OA) represents a sum of CCOA (coal combustion OA) and HOA. In panel (d) LO-OOA, MO-OOA, SV-OOA, and LV-OOA represent less oxidized OOA, more oxidized OOA, semi-volatile OOA, and low volatile OOA, respectively. TP-OOA and BG-OOA represent transported-OOA and background-OOA resolved in this study. TMB and IEPOX-SOA represent trimethylbenzene and Isoprene-epoxydiols-derived secondary organic aerosol, respectively. Lab. and Amb. represent studies from laboratories and field measurements of ambient air.
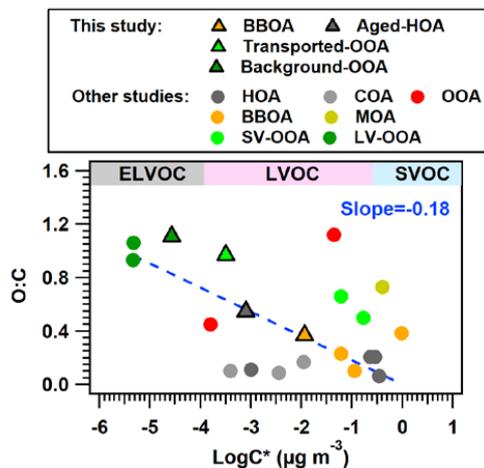
Figure 10. Scatter plot of O:C and average log C* from this and previous studies. MOA represents marine OA. The detailed
values in this plot are exhibited in Table S2–S5

3.5 Viscosity of OA

During this campaign, the predicted glass transmission temperature of OA ($T_{g,org}$) under dry conditions was 332.7 K, which is
in the range of ambient $T_{g,org}$ values estimated by Li et al. (2020b), and is much higher than the values (288.9–291.5 K)
estimated in the urban area of Beijing and at the rural site of Gucheng (Xu et al., 2021). It is consistent with the lower volatility
of OA in this study, where ~ 78 % (shown in Fig. 9 above) of OA were non-volatile compounds compared with 30–40 % in
Beijing and Gucheng (Xu et al., 2021).

The diurnal variations of OA viscosity as well as corresponding temperature and RH in previous and these studies are shown
in Figs. 11a and b. According to the viscosity categories (Reid et al., 2018), the ambient OA can exist in three phase states,
liquid ($\eta < 10^2$ Pa s), semisolid ($10^2 < \eta < 10^{12}$ Pa s), and amorphous solid ($\eta > 10^{12}$ Pa s). When $T_{g,org}$ is higher than the ambient
temperature, aerosol occurs as a solid phase, otherwise behaving as semisolid and liquid (Koop et al., 2011; Derieux et al.,
2018). The viscosity of ambient OA in this study generally ranged from 10^{-2} to 10^{22} pa s, which shows the OA phase exists
mainly as semi-solid (60 %), then followed by liquid (21 %, under high RH) and solid phases (19 %, low RH and high O:C).
As shown in Figs. 11a and b, the average daily fluctuation of RH could inversely affect the viscosity of OA, which stayed low
(5×10^2–10^6 pa s) during the nighttime and then increased during daytime, thereby reaching a solid phase state ($> 10^{12}$ pa s)
between 14:00–16:00. The variation of OA viscosity is similar to the diurnal variation of O:C. It is expected since higher O:C
due to photochemistry during the daytime leads to aerosol less volatile, which can result in a higher $T_{g,org}$, thus higher viscosity
(Shiraiwa et al., 2011; Mikhailov et al., 2009).

For fixed volatility and hygroscopicity (κ) of OA, ambient RH is the key parameter to determine the viscosity. We calculated
the RH-dependent viscosity based on the volatilities of different OA factors in Fig. 11. Compared with the deployed field
observations and laboratory experimental results, the predicted viscosities of two OOA factors are generally within the range
of viscosity values from ambient OOA summarized in Li et al. (2020b), and in the higher ranges of these from laboratory-
generated SOA summarized in Derieux et al. (2018). It is reasonable since the laboratory-generated SOA usually has a lower
viscosity due to a lower degree of oxidation (Aiken et al., 2008; Chen et al., 2015). Consistent with the inverse order of
volatility, OOA factors in this study undergo liquifying transition when the RH is above 67 % for transported OOA and 73 %
for background OOA. The viscosity curves of aged-HOA and BBOA as functions of RH are more viscous, which is consistent

with what has been found in other urban HOA (as the grey color tinted in Fig. 11c). Aged-HOA and BBOA in this study are more viscous on account of low f_{44} relative to the OOA factors, that is low hygroscopicity (Derieux et al., 2018). It suggests the phase transition RH would be higher when higher fractions of anthropogenic HOA and BBOA were involved in the particle.

510 Furthermore, we estimated the mixing time τ_{mix} (right axis in Fig. 11a) to roughly clarify the time scale of OA diffusion (Seinfeld and Pandis, 2016; Li and Shiraiwa, 2019) by assuming a uniform particle diameter of 200 nm for comparison with other studies conveniently. The results suggest the mixing time in OA varies dramatically from minutes at night to years in the afternoon. This large diurnal variation of OA mixing time might have significant impacts on aerosol evolution, such as gas-particle partitioning, multiphase chemical reactions, and nucleation, associated with the atmospheric fate of aerosols (Price et

515 al., 2016; Shiraiwa et al., 2011; Gržinić et al., 2015). The higher mixing time during the day indicates that the kinetic limitation of diffusion after aging processes may impede gas-particle partitioning, thus SOA formation and growth in ambient air (Xu et al., 2021; Galeazzo et al., 2021; Li and Shiraiwa, 2019). This result emphasizes the necessity of considering kinetical limit processes in the model, otherwise, the LVOC in the particle phase might be overpredicted (Renbaum-Wolff et al., 2013).
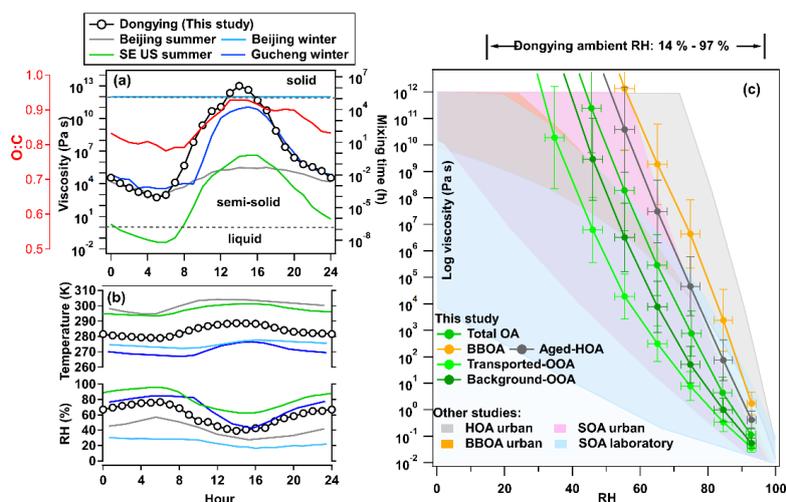
520 **Figure 11. Average diurnal variations of (a) estimated viscosity of total OA, (b) ambient RH and temperature in different studies; In addition to this study, Beijing and Gucheng reported by Xu et al. (2021) and southeastern United States (SE US) reported by Li et al. (2020b) were also shown. The mixing time assuming the particle size is 200 nm was also displayed in the right axis of panel (a) here. (c) Predicted viscosity of total OA, aged-HOA, BBOA, transported-OOA, and background-OOA as a function of RH. The ambient and laboratory viscosity results (Li et al., 2020b; Derieux et al., 2018) were also tinted in the background as a reference.**

525 **4 Conclusion**

To characterize the aging impact on sources, volatility, and viscosity of OA during the spring of 2018, a TD-AMS system was deployed in Dongying, a regional receptor site in North China Plain. The average PM_1 concentration was 31.5 ± 22.7 μg m^{-3}, of which secondary aerosols (inorganic + organic species) dominated in the entire campaign, accounting for nearly 86 % on average, which suggests the aging process plays an important role in the NCP urban outflows. Secondary inorganic aerosols

530 occupied 78 % of PM_1, which were mainly affected by south winds from urban areas in the NCP. Among secondary inorganic aerosols, nitrate accounted for the most (33 %), suggesting that nitrate and its precursor (NO_2) become the primary pollutants in the NCP area, which shall be considered in the regional pollution control in China.

Similar to previous studies (Xu et al., 2016; Cao et al., 2018; Huffman et al., 2009a; Xu et al., 2019), OA, as an integration of

different types of organic species, was moderately volatile in this study, where nitrate was the most volatile species and sulfate

535 was the least. Ambient inorganic aerosols all showed higher residuals upon heating at higher TD temperatures than their laboratory-derived pure standards, indicating the universal existence of low volatile metallic or organic-related species in ambient aerosols. This supports the complexity of ambient aerosols. Source apportionment of OA resolved four OA factors, BBOA (5 %), aged-HOA (28 %), transported-OOA (33 %), and background-OOA (33 %). BBOA, which was considered as emitted from the open fire nearby, is the most volatile in this study (average $C^* = 0.012$ µg m^{-3}). Aged-HOA was characterized

540 by high proportions of $C_xH_y^+$ ions and had good correlations with primary VOC species (benzene and ethyl toluene), as well as a pronounced peak of diurnal variations in the morning, suggesting that it is mainly transported from vehicle emissions from surrounding towns. The volatility of aged-HOA was impacted by the aging process, which has lower volatility (average $C^* = 8.1 \times 10^{-4}$ µg m^{-3}) than those of urban areas in NCP (Beijing), however still shows high SOA formation potential. In this study, total OOA (transported-OOA + background-OOA) accounted for the largest fractions of the OA (66 %) due to long-distance

545 aging and fewer effects from local emissions than those of urban areas. Generally, transported-OOA (average $C^* = 3.7 \times 10^{-4}$ µg m^{-3}) showed good agreements with secondary inorganic species, supporting their similar origins. Background-OOA showed the background concentration of OA in the outflow of the Chinese continent, which was around 2.6 µg m^{-3} on average. The background-OA was the least volatile factor in this study (average $C^* = 2.7 \times 10^{-5}$ µg m^{-3}), implying the existence of a large fraction of oligomers in this type of SOA and shall be further investigated. The results suggest the aging processes during the

550 transport of air plumes can significantly enhance the SOA formation and thus, decrease the OA volatility from different sources.

The glass transition temperature ($T_{g,org}$) and RH-dependent viscosity (η) of OA were predicted based on volatility distribution. The $T_{g,org}$ of total OA under dry conditions was 332.7 K, which is in the range of values from other campaigns, however much higher than those in urban NCP due to the low volatility of OA in our study (72 % of OA are non-volatile species). The viscosity of OA varied from 10^{-2} to 10^{22} Pa s, which mainly exist as semisolid particles. The solid phase usually occurred in the afternoon

555 time when the oxidation of OA was higher and RH was low. When the ambient RH was above 80 %, OA exists as liquid aerosols. Phase transition RH would be higher when higher fractions of anthropogenic HOA and BBOA were involved in the particle. The dynamic range of OA viscosity results in the mixing time of OA ranging from 10^{-4} to 10^6 h, suggesting a large timescale to reach equilibrium. This emphasizes the necessity to consider dynamic kinetic limits of OA viscosity when modeling OA evolutions. Note that the OA viscosity estimated here was mainly derived based on a method from the volatility

560 of pure organic compounds. there are also other factors that can influence OA viscosity in reality, e.g., OA functional group or molecular structure and organic/inorganic mixing state (Li et al., 2020b; Ditto et al., 2019), which shall be further investigated in the future. Overall, our results reveal how the aging process in the continental outflow can significantly influence the source and physiochemistry properties of OA, which shall be considered in the modeling and policy-making work regarding to evaluating its environment impact in the future.

565 *Data availability.* The data shown in the paper are available on request from the corresponding author (weiweihu@gig.ac.cn)

Author contributions. WH, WS, YS, designed the research. MZ, ZF, WD, XY, BY, SH, and HF conducted the field measurements. TF, YW, WH, YL, LH, CW, WC, MZ, ZF, and HF analyzed the data. TT and WC conducted the laboratory experiment on volatility. AP and FC supported the OA source analysis. WH and WC supported the viscosity analysis. TF and YW wrote the paper. WH, WC, CW, XH, LH, MS, XW, and AP reviewed and commented on the paper.

570 *Competing interests.* The authors declare that they have no conflict of interest.

Acknowledgments. This work was supported by National Natural Science Foundation of China (grant no. 41875156), State Environmental Protection Key Laboratory of Formation and Prevention of Urban Air Pollution Complex (no. 2021080540). Guangdong Pearl River Talents Program (2019QN01L948), Natural Science Foundation of Guangdong Province (grant no. 2019A1515011153),

575   Guangdong Foundation for Program of Science and Technology Research (Grant No.2020B1212060053), State Key Laboratory of Organic Geochemistry, GIGCAS (SKLOG2020-5, SKLOG2020-6). Bin Yuan was supported by the National Key R&D Plan of China (grant no. 2019YFE0106300), the National Natural Science Foundation of China (grant no. 41877302), and Guangdong Innovative and Entrepreneurial Research Team Program (grant no. 2016ZT06N263).

580 **References**

Aiken, A. C., de Foy, B., Wiedinmyer, C., DeCarlo, P. F., Ulbrich, I. M., Wehrli, M. N., Szidat, S., Prevot, A. S. H., Noda, J., Wacker, L., Volkamer, R., Fortner, E., Wang, J., Laskin, A., Shutthanandan, V., Zheng, J., Zhang, R., Paredes-Miranda, G., Arnott, W. P., Molina, L. T., Sosa, G., Querol, X., and Jimenez, J. L.: Mexico city aerosol analysis during MILAGRO using high resolution aerosol mass spectrometry at the urban supersite (T0) – Part 2: Analysis of the biomass burning contribution
585 and the non-fossil carbon fraction, Atmospheric Chemistry and Physics, 10, 5315-5341, 10.5194/acp-10-5315-2010, 2010.
Aiken, A. C., DeCarlo, P. F., Kroll, J. H., Worsnop, D. R., Huffman, J. A., Docherty, K. S., Ulbrich, I. M., Mohr, C., Kimmel, J. R., Sueper, D., Sun, Y., Zhang, Q., Trimborn, A., Northway, M., Ziemann, P. J., Canagaratna, M. R., Onasch, T. B., Alfarra, M. R., Prevot, A. S. H., Dommen, J., Duplissy, J., Metzger, A., Baltensperger, U., and Jimenez, J. L.: O/C and OM/OC Ratios of Primary, Secondary, and Ambient Organic Aerosols with High-Resolution Time-of-Flight Aerosol Mass
590 Spectrometry, Environmental Science & Technology, 42, 4478-4485, 10.1021/es703009q, 2008.
Aiken, A. C., Salcedo, D., Cubison, M. J., Huffman, J. A., DeCarlo, P. F., Ulbrich, I. M., Docherty, K. S., Sueper, D., Kimmel, J. R., Worsnop, D. R., Trimborn, A., Northway, M., Stone, E. A., Schauer, J. J., Volkamer, R. M., Fortner, E., de Foy, B., Wang, J., Laskin, A., Shutthanandan, V., Zheng, J., Zhang, R., Gaffney, J., Marley, N. A., Paredes-Miranda, G., Arnott, W. P., Molina, L. T., Sosa, G., and Jimenez, J. L.: Mexico City aerosol analysis during MILAGRO using high
595 resolution aerosol mass spectrometry at the urban supersite (T0) – Part 1: Fine particle composition and organic source apportionment, Atmos. Chem. Phys., 9, 6633-6653, 10.5194/acp-9-6633-2009, 2009.
An, W. J., Pathak, R. K., Lee, B.-H., and Pandis, S. N.: Aerosol volatility measurement using an improved thermodenuder: Application to secondary organic aerosol, Journal of Aerosol Science, 38, 305-314, 10.1016/j.jaerosci.2006.12.002, 2007.
Angell, C. A.: Relaxation in liquids, polymers and plastic crystals — strong/fragile patterns and problems, Journal of Non-
600 Crystalline Solids, 131-133, 13-31, https://doi.org/10.1016/0022-3093(91)90266-9, 1991.
Bertrand, A., Stefenelli, G., Jen, C. N., Pieber, S. M., Bruns, E. A., Ni, H., Temime-Roussel, B., Slowik, J. G., Goldstein, A. H., El Haddad, I., Baltensperger, U., Prévôt, A. S. H., Wortham, H., and Marchand, N.: Evolution of the chemical fingerprint of biomass burning organic aerosol during aging, Atmospheric Chemistry and Physics, 18, 7607-7624, 10.5194/acp-18-7607-2018, 2018.
605 Bianchi, F., Garmash, O., He, X., Yan, C., Iyer, S., Rosendahl, I., Xu, Z., Rissanen, M. P., Riva, M., Taipale, R., Sarnela, N., Petäjä, T., Worsnop, D. R., Kulmala, M., Ehn, M., and Junninen, H.: The role of highly oxygenated molecules (HOMs) in determining the composition of ambient ions in the boreal forest, Atmos. Chem. Phys., 17, 13819-13831, 10.5194/acp-17-13819-2017, 2017.
Cain, K. P. and Pandis, S. N.: A technique for the measurement of organic aerosol hygroscopicity, oxidation level, and
610 volatility distributions, Atmospheric Measurement Techniques, 10, 4865-4876, 10.5194/amt-10-4865-2017, 2017.
Canagaratna, M. R., Jimenez, J. L., Kroll, J. H., Chen, Q., Kessler, S. H., Massoli, P., Hildebrandt Ruiz, L., Fortner, E., Williams, L. R., Wilson, K. R., Surratt, J. D., Donahue, N. M., Jayne, J. T., and Worsnop, D. R.: Elemental ratio measurements of organic compounds using aerosol mass spectrometry: characterization, improved calibration, and implications, Atmospheric Chemistry and Physics, 15, 253-272, 10.5194/acp-15-253-2015, 2015.
615 Canagaratna, M. R., Jayne, J. T., Jimenez, J. L., Allan, J. D., Alfarra, M., Zhang, Q., Onasch, T. B., Drewnick, F., Coe, H., Middlebrook, A., Delia, A., Williams, L., Trimborn, A. M., Northway, M. J., DeCarlo, P., Kolb, C. E., Davidovcits, P., and Worsnop, D.: Chemical and microphysica characterization of ambient aerosols with the aerodyne aerosol mass spectrometer, Mass Spectrometry Reviews, 26, 185-222, 10.1002/mas.20115, 2007.
Canonaco, F., Crippa, M., Slowik, J. G., Baltensperger, U., and Prévôt, A. S. H.: SoFi, an IGOR-based interface for the
620 efficient use of the generalized multilinear engine (ME-2) for the source apportionment: ME-2 application to aerosol mass spectrometer data, Atmospheric Measurement Techniques, 6, 3649-3661, 10.5194/amt-6-3649-2013, 2013.

Cao, L.-M., Huang, X.-F., Li, Y.-Y., Hu, M., and He, L.-Y.: Volatility measurement of atmospheric submicron aerosols in an urban atmosphere in southern China, Atmospheric Chemistry and Physics, 18, 1729-1743, 10.5194/acp-18-1729-2018, 2018.

Cappa, C. D.: A model of aerosol evaporation kinetics in a thermodenuder, Atmos. Meas. Tech., 3, 579-592, 10.5194/amt-3-579-2010, 2010a.

Cappa, C. D.: A model of aerosol evaporation kinetics in a thermodenuder, Atmospheric Measurement Techniques, 3, 579-592, 10.5194/amt-3-579-2010, 2010b.

Cappa, C. D. and Jimenez, J. L.: Quantitative estimates of the volatility of ambient organic aerosol, Atmospheric Chemistry and Physics, 10, 5409-5424, 10.5194/acp-10-5409-2010, 2010.

Cerully, K. M., Bougiatioti, A., Hite, J. R., Guo, H., Xu, L., Ng, N. L., Weber, R., and Nenes, A.: On the link between hygroscopicity, volatility, and oxidation state of ambient and water-soluble aerosols in the southeastern United States, Atmospheric Chemistry and Physics, 15, 8679-8694, 10.5194/acp-15-8679-2015, 2015.

Champion, W. M., Rothfuss, N. E., Petters, M. D., and Grieshop, A. P.: Volatility and Viscosity Are Correlated in Terpene Secondary Organic Aerosol Formed in a Flow Reactor, Environmental Science & Technology Letters, 6, 513-519, 10.1021/acs.estlett.9b00412, 2019.

Chen, C., Zhang, H., Yan, W., Wu, N., Zhang, Q., and He, K.: Aerosol water content enhancement leads to changes in the major formation mechanisms of nitrate and secondary organic aerosols in winter over the North China Plain, Environ Pollut, 287, 117625, 10.1016/j.envpol.2021.117625, 2021a.

Chen, Q., Heald, C. L., Jimenez, J. L., Canagaratna, M. R., Zhang, Q., He, L. Y., Huang, X. F., Campuzano-Jost, P., Palm, B. B., Poulain, L., Kuwata, M., Martin, S. T., Abbatt, J. P. D., Lee, A. K. Y., and Liggio, J.: Elemental composition of organic aerosol: The gap between ambient and laboratory measurements, Geophysical Research Letters, 42, 4182-4189, 10.1002/2015gl063693, 2015.

Chen, W., Ye, Y., Hu, W., Zhou, H., Pan, T., Wang, Y., Song, W., Song, Q., Ye, C., Wang, C., Wang, B., Huang, S., Yuan, B., Zhu, M., Lian, X., Zhang, G., Bi, X., Jiang, F., Liu, J., Canonaco, F., Prevot, A. S. H., Shao, M., and Wang, X.: Real-time characterization of aerosol compositions, sources and aging processes in Guangzhou during PRIDE-GBA 2018 campaign, Journal of Geophysical Research: Atmospheres, 10.1029/2021jd035114, 2021b.

Chen, Y., Takeuchi, M., Nah, T., Xu, L., Canagaratna, M. R., Stark, H., Baumann, K., Canonaco, F., Prévôt, A. S. H., Huey, L. G., Weber, R. J., and Ng, N. L.: Chemical characterization of secondary organic aerosol at a rural site in the southeastern US: insights from simultaneous high-resolution time-of-flight aerosol mass spectrometer (HR-ToF-AMS) and FIGAERO chemical ionization mass spectrometer (CIMS) measurements, Atmospheric Chemistry and Physics, 20, 8421-8440, 10.5194/acp-20-8421-2020, 2020.

Chen, Y., Xu, L., Humphry, T., Hettiyadura, A. P. S., Ovadnevaite, J., Huang, S., Poulain, L., Schroder, J. C., Campuzano-Jost, P., Jimenez, J. L., Herrmann, H., O'Dowd, C., Stone, E. A., and Ng, N. L.: Response of the Aerodyne Aerosol Mass Spectrometer to Inorganic Sulfates and Organosulfur Compounds: Applications in Field and Laboratory Measurements, Environ Sci Technol, 53, 5176-5186, 10.1021/acs.est.9b00884, 2019.

Chow, J. C., Watson, J. G., Lowenthal, D. H., and Magliano, K. L.: Loss of PM2.5 nitrate from filter samples in central California, J Air Waste Manag Assoc, 55, 1158-1168, 10.1080/10473289.2005.10464704, 2005.

Claflin, M. S. and Ziemann, P. J.: Thermal desorption behavior of hemiacetal, acetal, ether, and ester oligomers, Aerosol Science and Technology, 53, 473-484, 10.1080/02786826.2019.1576853, 2019.

Cohen, M. D., Stunder, B. J. B., Rolph, G. D., Draxler, R. R., Stein, A. F., and Ngan, F.: NOAA's HYSPLIT Atmospheric Transport and Dispersion Modeling System, Bulletin of the American Meteorological Society, 96, 2059-2077, 10.1175/bams-d-14-00110.1, 2015.

Cubison, M. J., Ortega, A. M., Hayes, P. L., Farmer, D. K., Day, D., Lechner, M. J., Brune, W. H., Apel, E., Diskin, G. S., Fisher, J. A., Fuelberg, H. E., Hecobian, A., Knapp, D. J., Mikoviny, T., Riemer, D., Sachse, G. W., Sessions, W., Weber, R.

665   J., Weinheimer, A. J., Wisthaler, A., and Jimenez, J. L.: Effects of aging on organic aerosol from open biomass burning smoke in aircraft and laboratory studies, Atmospheric Chemistry and Physics, 11, 12049-12064, 10.5194/acp-11-12049-2011, 2011.

Daellenbach, K. R., Stefenelli, G., Bozzetti, C., Vlachou, A., Fermo, P., Gonzalez, R., Piazzalunga, A., Colombi, C., Canonaco, F., Hueglin, C., Kasper-Giebl, A., Jaffrezo, J.-L., Bianchi, F., Slowik, J. G., Baltensperger, U., El-Haddad, I., and

670   Prévôt, A. S. H.: Long-term chemical analysis and organic aerosol source apportionment at nine sites in central Europe: source identification and uncertainty assessment, Atmospheric Chemistry and Physics, 17, 13265-13282, 10.5194/acp-17-13265-2017, 2017.

Day, D. A., Campuzano-Jost, P., Nault, B. A., Palm, B. B., Hu, W., Guo, H., Wooldridge, P. J., Cohen, R. C., Docherty, K. S., Huffman, J. A., de Sá, S. S., Martin, S. T., and Jimenez, J. L.: A systematic re-evaluation of methods for quantification of

675   bulk particle-phase organic nitrates using real-time aerosol mass spectrometry, Atmospheric Measurement Techniques, 15, 459-483, 10.5194/amt-15-459-2022, 2022.

DeCarlo, P. F., Kimmel, J. R., Trimborn, A., Northway, M. J., Jayne, J. T., Aiken, A. C., Gonin, M., Fuhrer, K., Horvath, T., Docherty, K. S., Worsnop, D. R., and Jimenez, J. L.: Field-deployable, high-resolution, time-of-flight aerosol mass spectrometer, Anal Chem, 78, 8281-8289, 10.1021/ac061249n, 2006.

680   DeCarlo, P. F., Dunlea, E. J., Kimmel, J. R., Aiken, A. C., Sueper, D., Crounse, J., Wennberg, P. O., Emmons, L., Shinozuka, Y., Clarke, A., Zhou, J., Tomlinson, J., Collins, D. R., Knapp, D., Weinheimer, A. J., Montzka, D. D., Campos, T., and Jimenez, J. L.: Fast airborne aerosol size and chemistry measurements above Mexico City and Central Mexico during the MILAGRO campaign, Atmos. Chem. Phys., 8, 4027-4048, 10.5194/acp-8-4027-2008, 2008.

Denkenberger, K. A., Moffet, R. C., Holecek, J. C., Rebotier, T. P., and Prather, K. A.: Real-Time, Single-Particle

685   Measurements of Oligomers in Aged Ambient Aerosol Particles, Environmental Science & Technology, 41, 5439-5446, 10.1021/es070329l, 2007.

DeRieux, W.-S. W., Li, Y., Lin, P., Laskin, J., Laskin, A., Bertram, A. K., Nizkorodov, S. A., and Shiraiwa, M.: Predicting the glass transition temperature and viscosity of secondary organic material using molecular composition, Atmospheric Chemistry and Physics, 18, 6331-6351, 10.5194/acp-18-6331-2018, 2018.

690   Ditto, J. C., Joo, T., Khare, P., Sheu, R., Takeuchi, M., Chen, Y., Xu, W., Bui, A. A. T., Sun, Y., Ng, N. L., and Gentner, D. R.: Effects of Molecular-Level Compositional Variability in Organic Aerosol on Phase State and Thermodynamic Mixing Behavior, Environmental Science & Technology, 53, 13009-13018, 10.1021/acs.est.9b02664, 2019.

Docherty, K. S., Aiken, A. C., Huffman, J. A., Ulbrich, I. M., DeCarlo, P. F., Sueper, D., Worsnop, D. R., Snyder, D. C., Peltier, R. E., Weber, R. J., Grover, B. D., Eatough, D. J., Williams, B. J., Goldstein, A. H., Ziemann, P. J., and Jimenez, J. L.:

695   The 2005 Study of Organic Aerosols at Riverside (SOAR-1): instrumental intercomparisons and fine particle composition, Atmospheric Chemistry and Physics, 11, 12387-12420, 10.5194/acp-11-12387-2011, 2011.

Draxier, R. R. and Hess, G. D.: An overview of the HYSPLIT_4 modelling system for trajectories, dispersion and deposition, Aust Meteorol Mag, 47, 295-308, 1998.

Drewnick, F., Hings, S. S., DeCarlo, P., Jayne, J. T., Gonin, M., Fuhrer, K., Weimer, S., Jimenez, J. L., Demerjian, K. L.,

700   Borrmann, S., and Worsnop, D. R.: A New Time-of-Flight Aerosol Mass Spectrometer (TOF-AMS)—Instrument Description and First Field Deployment, Aerosol Science and Technology, 39, 637-658, 10.1080/02786820500182040, 2005.

Du, W., Sun, Y. L., Xu, Y. S., Jiang, Q., Wang, Q. Q., Yang, W., Wang, F., Bai, Z. P., Zhao, X. D., and Yang, Y. C.: Chemical characterization of submicron aerosol and particle growth events at a national background site (3295 m a.s.l.) on the Tibetan Plateau, Atmospheric Chemistry and Physics, 15, 10811-10824, 10.5194/acp-15-10811-2015, 2015.

705   Duan, J., Huang, R.-J., Li, Y., Chen, Q., Zheng, Y., Chen, Y., Lin, C., Ni, H., Wang, M., Ovadnevaite, J., Ceburnis, D., Chen, C., Worsnop, D. R., Hoffmann, T., O'Dowd, C., and Cao, J.: Summertime and wintertime atmospheric processes of secondary aerosol in Beijing, Atmospheric Chemistry and Physics, 20, 3793-3807, 10.5194/acp-20-3793-2020, 2020.

Ehn, M., Thornton, J. A., Kleist, E., Sipila, M., Junninen, H., Pullinen, I., Springer, M., Rubach, F., Tillmann, R., Lee, B., Lopez-Hilfiker, F., Andres, S., Acir, I. H., Rissanen, M., Jokinen, T., Schobesberger, S., Kangasluoma, J., Kontkanen, J.,
710 Nieminen, T., Kurten, T., Nielsen, L. B., Jorgensen, S., Kjaergaard, H. G., Canagaratna, M., Maso, M. D., Berndt, T., Petaja, T., Wahner, A., Kerminen, V. M., Kulmala, M., Worsnop, D. R., Wildt, J., and Mentel, T. F.: A large source of low-volatility secondary organic aerosol, Nature, 506, 476-479, 10.1038/nature13032, 2014.

Elser, M., Huang, R.-J., Wolf, R., Slowik, J. G., Wang, Q., Canonaco, F., Li, G., Bozzetti, C., Daellenbach, K. R., Huang, Y., Zhang, R., Li, Z., Cao, J., Baltensperger, U., El-Haddad, I., and Prévôt, A. S. H.: New insights into $PM_{2.5}$ chemical
715 composition and sources in two major cities in China during extreme haze events using aerosol mass spectrometry, Atmospheric Chemistry and Physics, 16, 3207-3225, 10.5194/acp-16-3207-2016, 2016.

Emanuelsson, E. U., Watne, A. K., Lutz, A., Ljungstrom, E., and Hallquist, M.: Influence of humidity, temperature, and radicals on the formation and thermal properties of secondary organic aerosol (SOA) from ozonolysis of beta-pinene, J Phys Chem A, 117, 10346-10358, 10.1021/jp4010218, 2013.

720 Epstein, S., Riipinen, I., and Donahue, N.: A Semiempirical Correlation between Enthalpy of Vaporization and Saturation Concentration for Organic Aerosol, Environmental science & technology, 44, 743-748, 10.1021/es902497z, 2009.

Evoy, E., Maclean, A. M., Rovelli, G., Li, Y., Tsimpidi, A. P., Karydis, V. A., Kamal, S., Lelieveld, J., Shiraiwa, M., Reid, J. P., and Bertram, A. K.: Predictions of diffusion rates of large organic molecules in secondary organic aerosols using the Stokes–Einstein and fractional Stokes–Einstein relations, Atmospheric Chemistry and Physics, 19, 10073-10085,
725 10.5194/acp-19-10073-2019, 2019.

Faulhaber, A. E., Thomas, B. M., Jimenez, J. L., Jayne, J. T., Worsnop, D. R., and Ziemann, P. J.: Characterization of a thermodenuder-particle beam mass spectrometer system for the study of organic aerosol volatility and composition, Atmos. Meas. Tech., 2, 15-31, 10.5194/amt-2-15-2009, 2009.

Fry, J. L., Draper, D. C., Zarzana, K. J., Campuzano-Jost, P., Day, D. A., Jimenez, J. L., Brown, S. S., Cohen, R. C., Kaser,
730 L., Hansel, A., Cappellin, L., Karl, T., Hodzic Roux, A., Turnipseed, A., Cantrell, C., Lefer, B. L., and Grossberg, N.: Observations of gas- and aerosol-phase organic nitrates at BEACHON-RoMBAS 2011, Atmospheric Chemistry and Physics, 13, 8585-8605, 10.5194/acp-13-8585-2013, 2013.

Galeazzo, T., Valorso, R., Li, Y., Camredon, M., Aumont, B., and Shiraiwa, M.: Estimation of secondary organic aerosol viscosity from explicit modeling of gas-phase oxidation of isoprene and α-pinene, Atmospheric Chemistry and Physics, 21,
735 10199-10213, 10.5194/acp-21-10199-2021, 2021.

Geng, G., Zhang, Q., Tong, D., Li, M., Zheng, Y., Wang, S., and He, K.: Chemical composition of ambient $PM_{2.5}$ over China and relationship to precursor emissions during 2005–2012, Atmospheric Chemistry and Physics, 17, 9187-9203, 10.5194/acp-17-9187-2017, 2017a.

Geng, G., Zhang, Q., Martin, R. V., Lin, J., Huo, H., Zheng, B., Wang, S., and He, K.: Impact of spatial proxies on the
740 representation of bottom-up emission inventories: A satellite-based analysis, Atmospheric Chemistry and Physics, 17, 4131-4145, 10.5194/acp-17-4131-2017, 2017b.

Gong, Z., Lan, Z., Xue, L., Zeng, L., He, L., and Huang, X.: Characterization of submicron aerosols in the urban outflow of the central Pearl River Delta region of China, Frontiers of Environmental Science & Engineering, 6, 725-733, 10.1007/s11783-012-0441-8, 2012.

745 Grieshop, A. P., Donahue, N. M., and Robinson, A. L.: Laboratory investigation of photochemical oxidation of organic aerosol from wood fires 2: analysis of aerosol mass spectrometer data, Atmos. Chem. Phys., 9, 2227-2240, 10.5194/acp-9-2227-2009, 2009a.

Grieshop, A. P., Logue, J. M., Donahue, N. M., and Robinson, A. L.: Laboratory investigation of photochemical oxidation of organic aerosol from wood fires 1: measurement and simulation of organic aerosol evolution, Atmos. Chem. Phys., 9, 1263-
750 1277, 10.5194/acp-9-1263-2009, 2009b.

Grieshop, A. P., Miracolo, M. A., Donahue, N. M., and Robinson, A. L.: Constraining the Volatility Distribution and Gas-Particle Partitioning of Combustion Aerosols Using Isothermal Dilution and Thermodenuder Measurements, Environmental Science & Technology, 43, 4750-4756, 10.1021/es8032378, 2009c.

Griffith, S. M., Huang, X. H. H., Louie, P. K. K., and Yu, J. Z.: Characterizing the thermodynamic and chemical composition factors controlling PM 2.5 nitrate: Insights gained from two years of online measurements in Hong Kong, Atmospheric Environment, 122, 864-875, 10.1016/j.atmosenv.2015.02.009, 2015.

Gržinić, G., Bartels-Rausch, T., Berkemeier, T., Türler, A., and Ammann, M.: Viscosity controls humidity dependence of N_2O_5 uptake to citric acid aerosol, Atmos. Chem. Phys., 15, 13615-13625, 10.5194/acp-15-13615-2015, 2015.

Hao, L. Q., Kortelainen, A., Romakkaniemi, S., Portin, H., Jaatinen, A., Leskinen, A., Komppula, M., Miettinen, P., Sueper, D., Pajunoja, A., Smith, J. N., Lehtinen, K. E. J., Worsnop, D. R., Laaksonen, A., and Virtanen, A.: Atmospheric submicron aerosol composition and particulate organic nitrate formation in a boreal forestland–urban mixed region, Atmospheric Chemistry and Physics, 14, 13483-13495, 10.5194/acp-14-13483-2014, 2014.

He, L.-Y., Huang, X.-F., Xue, L., Hu, M., Lin, Y., Zheng, J., Zhang, R., and Zhang, Y.-H.: Submicron aerosol analysis and organic source apportionment in an urban atmosphere in Pearl River Delta of China using high-resolution aerosol mass spectrometry, Journal of Geophysical Research, 116, 10.1029/2010jd014566, 2011.

Hering, S. and Cass, G.: The Magnitude of Bias in the Measurement of PM25 Arising from Volatilization of Particulate Nitrate from Teflon Filters, J Air Waste Manag Assoc, 49, 725-733, 10.1080/10473289.1999.10463843, 1999.

Hildebrandt, L., Engelhart, G. J., Mohr, C., Kostenidou, E., Lanz, V. A., Bougiatioti, A., DeCarlo, P. F., Prevot, A. S. H., Baltensperger, U., Mihalopoulos, N., Donahue, N. M., and Pandis, S. N.: Aged organic aerosol in the Eastern Mediterranean: the Finokalia Aerosol Measurement Experiment – 2008, Atmospheric Chemistry and Physics, 10, 4167-4186, 10.5194/acp-10-4167-2010, 2010.

Horowitz, L. W. and Jacob, D. J.: Global impact of fossil fuel combustion on atmospheric NOx, J Geophys Res-Atmos, 104, 23823-23840, Doi 10.1029/1999jd900205, 1999.

Hu, W., Hu, M., Hu, W.-W., Zheng, J., Chen, C., Wu, Y., and Guo, S.: Seasonal variations in high time-resolved chemical compositions, sources, and evolution of atmospheric submicron aerosols in the megacity Beijing, Atmospheric Chemistry and Physics, 17, 9979-10000, 10.5194/acp-17-9979-2017, 2017a.

Hu, W., Campuzano-Jost, P., Day, D. A., Croteau, P., Canagaratna, M. R., Jayne, J. T., Worsnop, D. R., and Jimenez, J. L.: Evaluation of the new capture vapourizer for aerosol mass spectrometers (AMS) through laboratory studies of inorganic species, Atmos. Meas. Tech., 10, 2897-2921, 10.5194/amt-10-2897-2017, 2017b.

Hu, W., Campuzano-Jost, P., Day, D. A., Croteau, P., Canagaratna, M. R., Jayne, J. T., Worsnop, D. R., and Jimenez, J. L.: Evaluation of the new capture vaporizer for aerosol mass spectrometers (AMS) through field studies of inorganic species, Aerosol Science and Technology, 51, 735-754, 10.1080/02786826.2017.1296104, 2017c.

Hu, W., Hu, M., Hu, W.-W., Niu, H., Zheng, J., Wu, Y., Chen, W., Chen, C., Li, L., Shao, M., Xie, S., and Zhang, Y.: Characterization of submicron aerosols influenced by biomass burning at a site in the Sichuan Basin, southwestern China, Atmospheric Chemistry and Physics, 16, 13213-13230, 10.5194/acp-16-13213-2016, 2016a.

Hu, W., Hu, M., Hu, W., Jimenez, J. L., Yuan, B., Chen, W., Wang, M., Wu, Y., Chen, C., Wang, Z., Peng, J., Zeng, L., and Shao, M.: Chemical composition, sources, and aging process of submicron aerosols in Beijing: Contrast between summer and winter, Journal of Geophysical Research: Atmospheres, 121, 1955-1977, 10.1002/2015jd024020, 2016b.

Hu, W., Palm, B. B., Day, D. A., Campuzano-Jost, P., Krechmer, J. E., Peng, Z., de Sá, S. S., Martin, S. T., Alexander, M. L., Baumann, K., Hacker, L., Kiendler-Scharr, A., Koss, A. R., de Gouw, J. A., Goldstein, A. H., Seco, R., Sjostedt, S. J., Park, J.-H., Guenther, A. B., Kim, S., Canonaco, F., Prévôt, A. S. H., Brune, W. H., and Jimenez, J. L.: Volatility and lifetime against OH heterogeneous reaction of ambient

isoprene-epoxydiols-derived secondary organic aerosol (IEPOX-SOA), Atmospheric Chemistry and Physics, 16, 11563-

795   11580, 10.5194/acp-16-11563-2016, 2016c.

Hu, W. W., Hu, M., Yuan, B., Jimenez, J. L., Tang, Q., Peng, J. F., Hu, W., Shao, M., Wang, M., Zeng, L. M., Wu, Y. S., Gong, Z. H., Huang, X. F., and He, L. Y.: Insights on organic aerosol aging and the influence of coal combustion at a regional receptor site of central eastern China, Atmospheric Chemistry and Physics, 13, 10095-10112, 10.5194/acp-13-10095-2013, 2013.

800   Huang, D. D., Li, Y. J., Lee, B. P., and Chan, C. K.: Analysis of organic sulfur compounds in atmospheric aerosols at the HKUST supersite in Hong Kong using HR-ToF-AMS, Environ Sci Technol, 49, 3672-3679, 10.1021/es5056269, 2015.

Huang, R.-J., He, Y., Duan, J., Li, Y., Chen, Q., Zheng, Y., Chen, Y., Hu, W., Lin, C., Ni, H., Dai, W., Cao, J., Wu, Y., Zhang, R., Xu, W., Ovadnevaite, J., Ceburnis, D., Hoffmann, T., and O'Dowd, C. D.: Contrasting sources and processes of particulate species in haze days with low and high relative humidity in wintertime Beijing, Atmospheric Chemistry and

805   Physics, 20, 9101-9114, 10.5194/acp-20-9101-2020, 2020.

Huang, X. F., He, L. Y., Hu, M., Canagaratna, M. R., Sun, Y., Zhang, Q., Zhu, T., Xue, L., Zeng, L. W., Liu, X. G., Zhang, Y. H., Jayne, J. T., Ng, N. L., and Worsnop, D. R.: Highly time-resolved chemical characterization of atmospheric submicron particles during 2008 Beijing Olympic Games using an Aerodyne High-Resolution Aerosol Mass Spectrometer, Atmospheric Chemistry and Physics, 10, 8933-8945, 10.5194/acp-10-8933-2010, 2010.

810   Huang, Y., Shen, H., Chen, H., Wang, R., Zhang, Y., Su, S., Chen, Y., Lin, N., Zhuo, S., Zhong, Q., Wang, X., Liu, J., Li, B., Liu, W., and Tao, S.: Quantification of global primary emissions of PM2.5, PM10, and TSP from combustion and industrial process sources, Environ Sci Technol, 48, 13834-13843, 10.1021/es503696k, 2014.

Huffman, J., Docherty, K., Aiken, A., Cubison, M., Ulbrich, I., DeCarlo, P., Sueper, D., Jayne, J., Worsnop, D., Ziemann, P., and Jimenez, J.: Chemically-resolved aerosol volatility measurements from two megacity field studies, Atmospheric

815   Chemistry and Physics, 9, 10.5194/acpd-9-2645-2009, 2009a.

Huffman, J. A., Ziemann, P. J., Jayne, J. T., Worsnop, D. R., and Jimenez, J. L.: Development and Characterization of a Fast-Stepping/Scanning Thermodenuder for Chemically-Resolved Aerosol Volatility Measurements, Aerosol Science and Technology, 42, 395-407, 10.1080/02786820802104981, 2008.

Huffman, J. A., Docherty, K. S., Mohr, C., Cubison, M. J., Ulbrich, I. M., Ziemann, P. J., Onasch, T. B., and Jimenez, J. L.:

820   Chemically-Resolved Volatility Measurements of Organic Aerosol from Different Sources, Environmental Science & Technology, 43, 5351-5357, 10.1021/es803539d, 2009b.

Isaacman-VanWertz, G. and Aumont, B.: Impact of organic molecular structure on the estimation of atmospherically relevant physicochemical parameters, Atmospheric Chemistry and Physics, 21, 6541-6563, 10.5194/acp-21-6541-2021, 2021.

Jayne, J. T., Leard, D. C., Zhang, X. F., Davidovits, P., Smith, K. A., Kolb, C. E., and Worsnop, D. R.: Development of an

825   aerosol mass spectrometer for size and composition analysis of submicron particles, Aerosol Sci Tech, 33, 49-70, 2000.

Jiang, Q., Sun, Y. L., Wang, Z., and Yin, Y.: Aerosol composition and sources during the Chinese Spring Festival: fireworks, secondary aerosol, and holiday effects, Atmospheric Chemistry and Physics, 15, 6023-6034, 10.5194/acp-15-6023-2015, 2015.

Jimenez, J. L., Jayne, J. T., Shi, Q., Kolb, C. E., Worsnop, D. R., Yourshaw, I., Seinfeld, J. H., Flagan, R. C., Zhang, X.,

830   Smith, K. A., Morris, J. W., and Davidovits, P.: Ambient aerosol sampling using the Aerodyne Aerosol Mass Spectrometer, Journal of Geophysical Research: Atmospheres, 108, https://doi.org/10.1029/2001JD001213, 2003.

Jimenez, J. L., Canagaratna, M. R., Donahue, N. M., Prevot, A. S. H., Zhang, Q., Kroll, J. H., DeCarlo, P. F., Allan, J. D., Coe, H., Ng, N. L., Aiken, A. C., Docherty, K. S., Ulbrich, I. M., Grieshop, A. P., Robinson, A. L., Duplissy, J., Smith, J. D., Wilson, K. R., Lanz, V. A., Hueglin, C., Sun, Y. L., Tian, J., Laaksonen, A., Raatikainen, T., Rautiainen, J., Vaattovaara, P.,

835   Ehn, M., Kulmala, M., Tomlinson, J. M., Collins, D. R., Cubison, M. J., Dunlea, E. J., Huffmam, J. A., Onasch, T. B., Alfarra, M. R., Williams, P. I., Bower, K., Kondo, Y., Schneider, J., Drewnick, F., Borrmann, S., Weimer, S., Demerjian, K.,

Salcedo, D., Cottrell, L., Griffin, R., Takami, A., Miyoshi, T., Hatakeyama, S., Shimono, A., Sun, J. Y., Zhang, Y. M., Dzepina, K., Kimmel, J. R., Sueper, D., Jayne, J. T., Herndon, S. C., Trimborn, A. M., Williams, L. R., Wood, E. C., Middlebrook, A. M., Kolb, C. E., Baltensperger, U., and Worsnop, D. R.: Evolution of Organic Aerosols in the Atmosphere,
840   Science, 2009.

Kang, H. G., Kim, Y., Collier, S., Zhang, Q., and Kim, H.: Volatility of Springtime ambient organic aerosol derived with thermodenuder aerosol mass spectrometry in Seoul, Korea, Environ Pollut, 304, 119203, 10.1016/j.envpol.2022.119203, 2022.

Karnezi, E., Riipinen, I., and Pandis, S. N.: Measuring the atmospheric organic aerosol volatility distribution: a theoretical
845   analysis, Atmospheric Measurement Techniques, 7, 2953-2965, 10.5194/amt-7-2953-2014, 2014.

Kolesar, K. R., Chen, C., Johnson, D., and Cappa, C. D.: The influences of mass loading and rapid dilution of secondary organic aerosol on particle volatility, Atmospheric Chemistry and Physics, 15, 9327-9343, 10.5194/acp-15-9327-2015, 2015.

Koop, T., Bookhold, J., Shiraiwa, M., and Pöschl, U.: Glass transition and phase state of organic compounds: dependency on molecular properties and implications for secondary organic aerosols in the atmosphere, Physical Chemistry Chemical
850   Physics, 13, 19238-19255, 10.1039/C1CP22617G, 2011.

Kostenidou, E., Karnezi, E., Hite Jr, J. R., Bougiatioti, A., Cerully, K., Xu, L., Ng, N. L., Nenes, A., and Pandis, S. N.: Organic aerosol in the summertime southeastern United States: components and their link to volatility distribution, oxidation state and hygroscopicity, Atmospheric Chemistry and Physics, 18, 5799-5819, 10.5194/acp-18-5799-2018, 2018.

Krechmer, J. E., Coggon, M. M., Massoli, P., Nguyen, T. B., Crounse, J. D., Hu, W., Day, D. A., Tyndall, G. S., Henze, D. K.,
855   Rivera-Rios, J. C., Nowak, J. B., Kimmel, J. R., Mauldin, R. L., 3rd, Stark, H., Jayne, J. T., Sipila, M., Junninen, H., Clair, J. M., Zhang, X., Feiner, P. A., Zhang, L., Miller, D. O., Brune, W. H., Keutsch, F. N., Wennberg, P. O., Seinfeld, J. H., Worsnop, D. R., Jimenez, J. L., and Canagaratna, M. R.: Formation of Low Volatility Organic Compounds and Secondary Organic Aerosol from Isoprene Hydroxyhydroperoxide Low-NO Oxidation, Environ Sci Technol, 49, 10330-10339, 10.1021/acs.est.5b02031, 2015.

860   Kroll, J. H. and Seinfeld, J. H.: Chemistry of secondary organic aerosol: Formation and evolution of low-volatility organics in the atmosphere, Atmospheric Environment, 42, 3593-3624, 10.1016/j.atmosenv.2008.01.003, 2008.

Kuwata, M., Zorn, S. R., and Martin, S. T.: Using elemental ratios to predict the density of organic material composed of carbon, hydrogen, and oxygen, Environ Sci Technol, 46, 787-794, 10.1021/es202525q, 2012.

Lee, B.-H., Pierce, J. R., Engelhart, G. J., and Pandis, S. N.: Volatility of secondary organic aerosol from the ozonolysis of
865   monoterpenes, Atmospheric Environment, 45, 2443-2452, 10.1016/j.atmosenv.2011.02.004, 2011.

Lee, B. P., Li, Y. J., Yu, J. Z., Louie, P. K. K., and Chan, C. K.: Characteristics of submicron particulate matter at the urban roadside in downtown Hong Kong-Overview of 4 months of continuous high-resolution aerosol mass spectrometer measurements, Journal of Geophysical Research: Atmospheres, 120, 7040-7058, 10.1002/2015jd023311, 2015.

Lee, Y., Huey, L. G., Wang, Y., Qu, H., Zhang, R., Ji, Y., Tanner, D. J., Wang, X., Tang, J., Song, W., Hu, W., and Zhang, Y.:
870   Photochemistry of Volatile Organic Compounds in the Yellow River Delta, China: Formation of O
3
and Peroxyacyl Nitrates, Journal of Geophysical Research: Atmospheres, 126, 10.1029/2021jd035296, 2021.

Lei, Y., Zhang, Q., Nielsen, C., and He, K.: An inventory of primary air pollutants and CO2 emissions from cement production in China, 1990–2020, Atmospheric Environment, 45, 147-154, 10.1016/j.atmosenv.2010.09.034, 2011.

875   Li, H., Cheng, J., Zhang, Q., Zheng, B., Zhang, Y., Zheng, G., and He, K.: Rapid transition in winter aerosol composition in Beijing from 2014 to 2017: response to clean air actions, Atmospheric Chemistry and Physics, 19, 11485-11499, 10.5194/acp-19-11485-2019, 2019.

Li, H., Zhang, Q., Zheng, B., Chen, C., Wu, N., Guo, H., Zhang, Y., Zheng, Y., Li, X., and He, K.: Nitrate-driven urban haze pollution during summertime over the North China Plain, Atmospheric Chemistry and Physics, 18, 5293-5306, 10.5194/acp-

880   18-5293-2018, 2018.

Li, H., Zhang, Q., Zhang, Q., Chen, C., Wang, L., Wei, Z., Zhou, S., Parworth, C., Zheng, B., Canonaco, F., Prévôt, A. S. H., Chen, P., Zhang, H., Wallington, T. J., and He, K.: Wintertime aerosol chemistry and haze evolution in an extremely polluted city of the North China Plain: significant contribution from coal and biomass combustion, Atmospheric Chemistry and Physics, 17, 4751-4768, 10.5194/acp-17-4751-2017, 2017a.

885   Li, J., Liu, Z., Cao, L., Gao, W., Yan, Y., Mao, J., Zhang, X., He, L., Xin, J., Tang, G., Ji, D., Hu, B., Wang, L., Wang, Y., Dai, L., Zhao, D., Du, W., and Wang, Y.: Highly time-resolved chemical characterization and implications of regional transport for submicron aerosols in the North China Plain, Sci Total Environ, 705, 135803, 10.1016/j.scitotenv.2019.135803, 2020a.

Li, M., Zhang, Q., Kurokawa, J.-i., Woo, J.-H., He, K., Lu, Z., Ohara, T., Song, Y., Streets, D. G., Carmichael, G. R., Cheng, Y., Hong, C., Huo, H., Jiang, X., Kang, S., Liu, F., Su, H., and Zheng, B.: MIX: a mosaic Asian anthropogenic emission

890   inventory under the international collaboration framework of the MICS-Asia and HTAP, Atmospheric Chemistry and Physics, 17, 935-963, 10.5194/acp-17-935-2017, 2017b.

Li, W., Shao, L., Shi, Z., Chen, J., Yang, L., Yuan, Q., Yan, C., Zhang, X., Wang, Y., Sun, J., Zhang, Y., Shen, X., Wang, Z., and Wang, W.: Mixing state and hygroscopicity of dust and haze particles before leaving Asian continent, Journal of Geophysical Research: Atmospheres, 119, 1044-1059, 10.1002/2013jd021003, 2014.

895   Li, X., Dallmann, T. R., May, A. A., Tkacik, D. S., Lambe, A. T., Jayne, J. T., Croteau, P. L., and Presto, A. A.: Gas-Particle Partitioning of Vehicle Emitted Primary Organic Aerosol Measured in a Traffic Tunnel, Environ Sci Technol, 50, 12146-12155, 10.1021/acs.est.6b01666, 2016a.

Li, Y. and Shiraiwa, M.: Timescales of secondary organic aerosols to reach equilibrium at various temperatures and relative humidities, Atmospheric Chemistry and Physics, 19, 5959-5971, 10.5194/acp-19-5959-2019, 2019.

900   Li, Y., Pöschl, U., and Shiraiwa, M.: Molecular corridors and parameterizations of volatility in the chemical evolution of organic aerosols, Atmospheric Chemistry and Physics, 16, 3327-3344, 10.5194/acp-16-3327-2016, 2016b.

Li, Y., Day, D. A., Stark, H., Jimenez, J. L., and Shiraiwa, M.: Predictions of the glass transition temperature and viscosity of organic aerosols from volatility distributions, Atmospheric Chemistry and Physics, 20, 8103-8122, 10.5194/acp-20-8103-2020, 2020b.

905   Li, Y. J., Lee, B. P., Su, L., Fung, J. C. H., and Chan, C. K.: Seasonal characteristics of fine particulate matter (PM) based on high-resolution time-of-flight aerosol mass spectrometric (HR-ToF-AMS) measurements at the HKUST Supersite in Hong Kong, Atmospheric Chemistry and Physics, 15, 37-53, 10.5194/acp-15-37-2015, 2015.

Liang, L., Engling, G., Liu, C., Xu, W., Liu, X., Cheng, Y., Du, Z., Zhang, G., Sun, J., and Zhang, X.: Measurement report: Chemical characteristics of $PM_{2.5}$ during typical biomass burning season at an agricultural site of the North China Plain,

910   Atmospheric Chemistry and Physics, 21, 3181-3192, 10.5194/acp-21-3181-2021, 2021.

Liu, J., Li, J., and Yao, F.: Source-receptor relationship of transboundary particulate matter pollution between China, South Korea and Japan: Approaches, current understanding and limitations, Critical Reviews in Environmental Science and Technology, 1-25, 10.1080/10643389.2021.1964308, 2021.

Liu, Y., Wu, Z., Wang, Y., Xiao, Y., Gu, F., Jing Zheng, Tianyi Tan, Shang, D., Wu, Y., Zeng, L., Min Hu, Adam Bateman,

915   and Martin, S. T.: Sub-micrometer Particles are in the Liquid State during Heavy Haze Episodes in the Urban Atmosphere of Beijing, China, environmental Science & Technology Letters, 10.1021/acs.estlett.7b00352, 2017.

Lopez-Hilfiker, F. D., Pospisilova, V., Huang, W., Kalberer, M., Mohr, C., Stefenelli, G., Thornton, J. A., Baltensperger, U., Prevot, A. S. H., and Slowik, J. G.: An extractive electrospray ionization time-of-flight mass spectrometer (EESI-TOF) for online measurement of atmospheric aerosol particles, Atmospheric Measurement Techniques, 12, 4867-4886, 10.5194/amt-

920   12-4867-2019, 2019.

Lopez-Hilfiker, F. D., Mohr, C., D'Ambro, E. L., Lutz, A., Riedel, T. P., Gaston, C. J., Iyer, S., Zhang, Z., Gold, A., Surratt, J. D., Lee, B. H., Kurten, T., Hu, W. W., Jimenez, J., Hallquist, M., and Thornton, J. A.: Molecular Composition and Volatility

of Organic Aerosol in the Southeastern U.S.: Implications for IEPOX Derived SOA, Environ Sci Technol, 50, 2200-2209, 10.1021/acs.est.5b04769, 2016.

925   Louvaris, E. E., Karnezi, E., Kostenidou, E., Kaltsonoudis, C., and Pandis, S. N.: Estimation of the volatility distribution of organic aerosol combining thermodenuder and isothermal dilution measurements, Atmospheric Measurement Techniques, 10, 3909-3918, 10.5194/amt-10-3909-2017, 2017a.

Louvaris, E. E., Florou, K., Karnezi, E., Papanastasiou, D. K., Gkatzelis, G. I., and Pandis, S. N.: Volatility of source apportioned wintertime organic aerosol in the city of Athens, Atmospheric Environment, 158, 138-147,

930   10.1016/j.atmosenv.2017.03.042, 2017b.

Maclean, A. M., Li, Y., Crescenzo, G. V., Smith, N. R., Karydis, V. A., Tsimpidi, A. P., Butenhoff, C. L., Faiola, C. L., Lelieveld, J., Nizkorodov, S. A., Shiraiwa, M., and Bertram, A. K.: Global Distribution of the Phase State and Mixing Times within Secondary Organic Aerosol Particles in the Troposphere Based on Room-Temperature Viscosity Measurements, ACS Earth and Space Chemistry, 10.1021/acsearthspacechem.1c00296, 2021.

935   May, A. A., Presto, A. A., Hennigan, C. J., Nguyen, N. T., Gordon, T. D., and Robinson, A. L.: Gas-particle partitioning of primary organic aerosol emissions: (1) Gasoline vehicle exhaust, Atmospheric Environment, 77, 128-139, 10.1016/j.atmosenv.2013.04.060, 2013a.

May, A. A., Presto, A. A., Hennigan, C. J., Nguyen, N. T., Gordon, T. D., and Robinson, A. L.: Gas-particle partitioning of primary organic aerosol emissions: (2) diesel vehicles, Environ Sci Technol, 47, 8288-8296, 10.1021/es400782j, 2013b.

940   May, A. A., Levin, E. J. T., Hennigan, C. J., Riipinen, I., Lee, T., Collett, J. L., Jimenez, J. L., Kreidenweis, S. M., and Robinson, A. L.: Gas-particle partitioning of primary organic aerosol emissions: 3. Biomass burning, Journal of Geophysical Research: Atmospheres, 118, 11,327-311,338, 10.1002/jgrd.50828, 2013c.

Mei, F., Setyan, A., Zhang, Q., and Wang, J.: CCN activity of organic aerosols observed downwind of urban emissions during CARES, Atmospheric Chemistry and Physics, 13, 12155-12169, 10.5194/acp-13-12155-2013, 2013.

945   Middlebrook, A. M., Bahreini, R., Jimenez, J. L., and Canagaratna, M. R.: Evaluation of Composition-Dependent Collection Efficiencies for the Aerodyne Aerosol Mass Spectrometer using Field Data, Aerosol Science and Technology, 46, 258-271, 10.1080/02786826.2011.620041, 2012.

Mikhailov, E., Vlasenko, S., Martin, S. T., Koop, T., and Pöschl, U.: Amorphous and crystalline aerosol particles interacting with water vapor: conceptual framework and experimental evidence for restructuring, phase transitions and kinetic

950   limitations, atmos Chem Phys, 2009.

Moffet, R. C., Foy, B. d., Molina, L. T., Molina, M. J., and Prather, K. A.: Measurement of ambient aerosols in northern Mexico City by single particle mass spectrometry, Atmos Chem Phys, 2008.

Mohr, C., DeCarlo, P. F., Heringa, M. F., Chirico, R., Slowik, J. G., Richter, R., Reche, C., Alastuey, A., Querol, X., Seco, R., Peñuelas, J., Jiménez, J. L., Crippa, M., Zimmermann, R., Baltensperger, U., and Prévôt, A. S. H.: Identification and

955   quantification of organic aerosol from cooking and other sources in Barcelona using aerosol mass spectrometer data, Atmospheric Chemistry and Physics, 12, 1649-1665, 10.5194/acp-12-1649-2012, 2012.

Ng, N. L., Canagaratna, M. R., Jimenez, J. L., Chhabra, P. S., Seinfeld, J. H., and Worsnop, D. R.: Changes in organic aerosol composition with aging inferred from aerosol mass spectra, Atmospheric Chemistry and Physics, 11, 6465-6474, 10.5194/acp-11-6465-2011, 2011a.

960   Ng, N. L., Canagaratna, M. R., Jimenez, J. L., Zhang, Q., Ulbrich, I. M., and Worsnop, D. R.: Real-Time Methods for Estimating Organic Component Mass Concentrations from Aerosol Mass Spectrometer Data, Environmental Science & Technology, 45, 910-916, 10.1021/es102951k, 2011b.

Ng, N. L., Canagaratna, M. R., Zhang, Q., Jimenez, J. L., Tian, J., Ulbrich, I. M., Kroll, J. H., Docherty, K. S., Chhabra, P. S., Bahreini, R., Murphy, S. M., Seinfeld, J. H., Hildebrandt, L., Donahue, N. M., DeCarlo, P. F., Lanz, V. A., Prévôt, A. S. H.,

965   Dinar, E., Rudich, Y., and Worsnop, D. R.: Organic aerosol components observed in Northern Hemispheric datasets from

Aerosol Mass Spectrometry, Atmospheric Chemistry and Physics, 10, 4625-4641, 10.5194/acp-10-4625-2010, 2010.

Paciga, A., Karnezi, E., Kostenidou, E., Hildebrandt, L., Psichoudaki, M., Engelhart, G. J., Lee, B.-H., Crippa, M., Prévôt, A. S. H., Baltensperger, U., and Pandis, S. N.: Volatility of organic aerosol and its components in the megacity of Paris, Atmospheric Chemistry and Physics, 16, 2013-2023, 10.5194/acp-16-2013-2016, 2016.

970 Park, S. H., Rogak, S. N., and Grieshop, A. P.: A Two-Dimensional Laminar Flow Model for Thermodenuders Applied to Vapor Pressure Measurements, Aerosol Science and Technology, 47, 283-293, 10.1080/02786826.2012.750711, 2012.

Petit, J. E., Favez, O., Albinet, A., and Canonaco, F.: A user-friendly tool for comprehensive evaluation of the geographical origins of atmospheric pollution: Wind and trajectory analyses, Environ Modell Softw, 88, 183-187, https://doi.org/10.1016/j.envsoft.2016.11.022, 2017.

975 Pieber, S. M., El Haddad, I., Slowik, J. G., Canagaratna, M. R., Jayne, J. T., Platt, S. M., Bozzetti, C., Daellenbach, K. R., Fröhlich, R., Vlachou, A., Klein, F., Dommen, J., Miljevic, B., Jiménez, J. L., Worsnop, D. R., Baltensperger, U., and Prévôt, A. S. H.: Inorganic Salt Interference on CO2+ in Aerodyne AMS and ACSM Organic Aerosol Composition Studies, Environ Sci Technol, 50, 10494–10503, 10.1021/acs.est.6b01035, 2016.

Polissar, A. V., Hopke, P. K., Paatero, P., Kaufmann, Y. J., Hall, D. K., Bodhaine, B. A., Dutton, E. G., and Harris, J. M.: The
980 aerosol at Barrow, Alaska: long-term trends and source locations, Atmospheric Environment, 33, 2441-2458, Doi 10.1016/S1352-2310(98)00423-3, 1999.

Price, H. C., Mattsson, J., and Murray, B. J.: Sucrose diffusion in aqueous solution, Phys Chem Chem Phys, 18, 19207-19216, 10.1039/c6cp03238a, 2016.

Qin, Y. M., Tan, H. B., Li, Y. J., Schurman, M. I., Li, F., Canonaco, F., Prévôt, A. S. H., and Chan, C. K.: Impacts of traffic
985 emissions on atmospheric particulate nitrate and organics at a downwind site on the periphery of Guangzhou, China, Atmospheric Chemistry and Physics, 17, 10245-10258, 10.5194/acp-17-10245-2017, 2017.

Quan, J., Zhang, Q., He, H., Liu, J., Huang, M., and Jin, H.: Analysis of the formation of fog and haze in North China Plain (NCP), Atmospheric Chemistry and Physics, 11, 8205-8214, 10.5194/acp-11-8205-2011, 2011.

Reid, J. P., Bertram, A. K., Topping, D. O., Laskin, A., Martin, S. T., Petters, M. D., Pope, F. D., and Rovelli, G.: The
990 viscosity of atmospherically relevant organic particles, Nat Commun, 9, 956, 10.1038/s41467-018-03027-z, 2018.

Renbaum-Wolff, L., Grayson, J. W., Bateman, A. P., Kuwata, M., Sellier, M., Murray, B. J., Shilling, J. E., Martin, S. T., and Bertram, A. K.: Viscosity of alpha-pinene secondary organic material and implications for particle growth and reactivity, Proc Natl Acad Sci U S A, 110, 8014-8019, 10.1073/pnas.1219548110, 2013.

Riipinen, I., Pierce, J. R., Donahue, N. M., and Pandis, S. N.: Equilibration time scales of organic aerosol inside
995 thermodenuders: Evaporation kinetics versus thermodynamics, Atmospheric Environment, 44, 597-607, 10.1016/j.atmosenv.2009.11.022, 2010.

Saha, P. K. and Grieshop, A. P.: Exploring Divergent Volatility Properties from Yield and Thermodenuder Measurements of Secondary Organic Aerosol from alpha-Pinene Ozonolysis, Environ Sci Technol, 50, 5740-5749, 10.1021/acs.est.6b00303, 2016.

1000 Saha, P. K., Khlystov, A., and Grieshop, A. P.: Determining Aerosol Volatility Parameters Using a "Dual Thermodenuder" System: Application to Laboratory-Generated Organic Aerosols, Aerosol Science and Technology, 49, 620-632, 10.1080/02786826.2015.1056769, 2015.

Saha, P. K., Khlystov, A., and Grieshop, A. P.: Downwind evolution of the volatility and mixing state of near-road aerosols near a US interstate highway, Atmospheric Chemistry and Physics, 18, 2139-2154, 10.5194/acp-18-2139-2018, 2018.

1005 Saha, P. K., Khlystov, A., Yahya, K., Zhang, Y., Xu, L., Ng, N. L., and Grieshop, A. P.: Quantifying the volatility of organic aerosol in the southeastern US, Atmospheric Chemistry and Physics, 17, 501-520, 10.5194/acp-17-501-2017, 2017.

Sato, K., Fujitani, Y., Inomata, S., Morino, Y., Tanabe, K., Hikida, T., Shimono, A., Takami, A., Fushimi, A., Kondo, Y., Imamura, T., Tanimoto, H., and Sugata, S.: A study of volatility by composition, heating, and dilution measurements of

secondary organic aerosol from 1,3,5-trimethylbenzene, Atmospheric Chemistry and Physics, 19, 14901-14915,

1010 10.5194/acp-19-14901-2019, 2019.

Sato, K., Fujitani, Y., Inomata, S., Morino, Y., Tanabe, K., Ramasamy, S., Hikida, T., Shimono, A., Takami, A., Fushimi, A., Kondo, Y., Imamura, T., Tanimoto, H., and Sugata, S.: Studying volatility from composition, dilution, and heating measurements of secondary organic aerosols formed during α-pinene ozonolysis, Atmospheric Chemistry and Physics, 18, 5455-5466, 10.5194/acp-18-5455-2018, 2018.

1015 Seinfeld, J. H. and Pandis, S. N.: Atmospheric chemistry and physics - from air pollution to climate change_Third Edition., 2016.

Shiraiwa, M. and Seinfeld, J. H.: Equilibrium timescale of atmospheric secondary organic aerosol partitioning, Geophysical Research Letters, 39, 10.1029/2012gl054008, 2012.

Shiraiwa, M., Ammann, M., Koop, T., and Poschl, U.: Gas uptake and chemical aging of semisolid organic aerosol particles,

1020 Proc Natl Acad Sci U S A, 108, 11003-11008, 10.1073/pnas.1103045108, 2011.

Shiraiwa, M., Pfrang, C., Koop, T., and Pöschl, U.: Kinetic multi-layer model of gas-particle interactions in aerosols and clouds (KM-GAP): linking condensation, evaporation and chemical reactions of organics, oxidants and water, Atmospheric Chemistry and Physics, 12, 2777-2794, 10.5194/acp-12-2777-2012, 2012.

Shiraiwa, M., Li, Y., Tsimpidi, A. P., Karydis, V. A., Berkemeier, T., Pandis, S. N., Lelieveld, J., Koop, T., and Pöschl, U.:

1025 Global distribution of particle phase state in atmospheric secondary organic aerosols, Nature Communications, 8, 10.1038/ncomms15002, 2017.

Song, Z., Fu, D., Zhang, X., Wu, Y., Xia, X., He, J., Han, X., Zhang, R., and Che, H.: Diurnal and seasonal variability of PM2.5 and AOD in North China plain: Comparison of MERRA-2 products and ground measurements, Atmospheric Environment, 191, 70-78, 10.1016/j.atmosenv.2018.08.012, 2018.

1030 Squizzato, S., Masiol, M., Innocente, E., Pecorari, E., Rampazzo, G., and Pavoni, B.: A procedure to assess local and long-range transport contributions to PM2.5 and secondary inorganic aerosol, Journal of Aerosol Science, 46, 64-76, 10.1016/j.jaerosci.2011.12.001, 2012.

Sun, J., Huang, L., Liao, H., Li, J., and Hu, J.: Impacts of Regional Transport on Particulate Matter Pollution in China: a Review of Methods and Results, Current Pollution Reports, 3, 182-191, 10.1007/s40726-017-0065-5, 2017.

1035 Sun, Y., Jiang, Q., Wang, Z., Fu, P., Li, J., Yang, T., and Yin, Y.: Investigation of the sources and evolution processes of severe haze pollution in Beijing in January 2013, Journal of Geophysical Research: Atmospheres, 119, 4380-4398, 10.1002/2014jd021641, 2014.

Sun, Y., Wang, Z., Dong, H., Yang, T., Li, J., Pan, X., Chen, P., and Jayne, J. T.: Characterization of summer organic and inorganic aerosols in Beijing, China with an Aerosol Chemical Speciation Monitor, Atmospheric Environment, 51, 250-259,

1040 10.1016/j.atmosenv.2012.01.013, 2012.

Sun, Y., Chen, C., Zhang, Y., Xu, W., Zhou, L., Cheng, X., Zheng, H., Ji, D., Li, J., Tang, X., Fu, P., and Wang, Z.: Rapid formation and evolution of an extreme haze episode in Northern China during winter 2015, Sci Rep, 6, 27151, 10.1038/srep27151, 2016.

Sun, Y. L., Wang, Z. F., Fu, P. Q., Yang, T., Jiang, Q., Dong, H. B., Li, J., and Jia, J. J.: Aerosol composition, sources and

1045 processes during wintertime in Beijing, China, Atmospheric Chemistry and Physics, 13, 4577-4592, 10.5194/acp-13-4577-2013, 2013.

Sun, Y. L., Wang, Z. F., Du, W., Zhang, Q., Wang, Q. Q., Fu, P. Q., Pan, X. L., Li, J., Jayne, J., and Worsnop, D. R.: Long-term real-time measurements of aerosol particle composition in Beijing, China: seasonal variations, meteorological effects, and source analysis, Atmospheric Chemistry and Physics, 15, 10149-10165, 10.5194/acp-15-10149-2015, 2015.

1050 Ulbrich, I. M., Canagaratna, M. R., Zhang, Q., Worsnop, D. R., and Jimenez, J. L.: Interpretation of organic components from Positive Matrix Factorization of aerosol mass spectrometric data, Atmos. Chem. Phys., 9, 2891-2918, 10.5194/acp-9-

2891-2009, 2009.

Virtanen, A., Joutsensaari, J., Koop, T., Kannosto, J., Yli-Pirila, P., Leskinen, J., Makela, J. M., Holopainen, J. K., Poschl, U., Kulmala, M., Worsnop, D. R., and Laaksonen, A.: An amorphous solid state of biogenic secondary organic aerosol particles,

1055   Nature, 467, 824-827, 10.1038/nature09455, 2010.

Vlachou, A., Tobler, A., Lamkaddam, H., Canonaco, F., Daellenbach, K. R., Jaffrezo, J.-L., Minguillón, M. C., Maasikmets, M., Teinemaa, E., Baltensperger, U., El Haddad, I., and Prévôt, A. S. H.: Development of a versatile source apportionment analysis based on positive matrix factorization: a case study of the seasonal variation of organic aerosol sources in Estonia, Atmospheric Chemistry and Physics, 19, 7279-7295, 10.5194/acp-19-7279-2019, 2019.

1060   Waked, A., Favez, O., Alleman, L. Y., Piot, C., Petit, J. E., Delaunay, T., Verlinden, E., Golly, B., Besombes, J. L., Jaffrezo, J. L., and Leoz-Garziandia, E.: Source apportionment of PM$_{10}$ in a north-western Europe regional urban background site (Lens, France) using positive matrix factorization and including primary biogenic emissions, Atmospheric Chemistry and Physics, 14, 3325-3346, 10.5194/acp-14-3325-2014, 2014.

Wang, Q., Sun, Y., Jiang, Q., Du, W., Sun, C., Fu, P., and Wang, Z.: Chemical composition of aerosol particles and light

1065   extinction apportionment before and during the heating season in Beijing, China, Journal of Geophysical Research: Atmospheres, 120, 12708-12722, 10.1002/2015jd023871, 2015.

Wang, Y., Chen, Y., Wu, Z., Shang, D., Bian, Y., Du, Z., Schmitt, S. H., Su, R., Gkatzelis, G. I., Schlag, P., Hohaus, T., Voliotis, A., Lu, K., Zeng, L., Zhao, C., Alfarra, M. R., McFiggans, G., Wiedensohler, A., Kiendler-Scharr, A., Zhang, Y., and Hu, M.: Mutual promotion between aerosol particle liquid water and particulate nitrate enhancement leads to severe nitrate-

1070   dominated particulate matter pollution and low visibility, Atmospheric Chemistry and Physics, 20, 2161-2175, 10.5194/acp-20-2161-2020, 2020.

Xie, Y., Wang, G., Wang, X., Chen, J., Chen, Y., Tang, G., Wang, L., Ge, S., Xue, G., Wang, Y., and Gao, J.: Nitrate-dominated PM$_{2.5}$ and elevation of particle pH observed in urban Beijing during the winter of 2017, Atmospheric Chemistry and Physics, 20, 5019-5033, 10.5194/acp-20-5019-2020, 2020.

1075   Xu, L., Williams, L. R., Young, D. E., Allan, J. D., Coe, H., Massoli, P., Fortner, E., Chhabra, P., Herndon, S., Brooks, W. A., Jayne, J. T., Worsnop, D. R., Aiken, A. C., Liu, S., Gorkowski, K., Dubey, M. K., Fleming, Z. L., Visser, S., Prévôt, A. S. H., and Ng, N. L.: Wintertime aerosol chemical composition, volatility, and spatial variability in the greater London area, Atmospheric Chemistry and Physics, 16, 1139-1160, 10.5194/acp-16-1139-2016, 2016.

Xu, P., Zhang, J., Ji, D., Liu, Z., Tang, G., Jiang, C., and Wang, Y.: Characterization of submicron particles during autumn in

1080   Beijing, China, J Environ Sci (China), 63, 16-27, 10.1016/j.jes.2017.03.036, 2018.

Xu, W., Han, T., Du, W., Wang, Q., Chen, C., Zhao, J., Zhang, Y., Li, J., Fu, P., Wang, Z., Worsnop, D. R., and Sun, Y.: Effects of Aqueous-Phase and Photochemical Processing on Secondary Organic Aerosol Formation and Evolution in Beijing, China, Environ Sci Technol, 51, 762-770, 10.1021/acs.est.6b04498, 2017.

Xu, W., Chen, C., Qiu, Y., Li, Y., Zhang, Z., Karnezi, E., Pandis, S. N., Xie, C., Li, Z., Sun, J., Ma, N., Xu, W., Fu, P., Wang,

1085   Z., Zhu, J., Worsnop, D. R., Ng, N. L., and Sun, Y.: Organic aerosol volatility and viscosity in the North China Plain: contrast between summer and winter, Atmospheric Chemistry and Physics, 21, 5463-5476, 10.5194/acp-21-5463-2021, 2021.

Xu, W., Xie, C., Karnezi, E., Zhang, Q., Wang, J., Pandis, S. N., Ge, X., Zhang, J., An, J., Wang, Q., Zhao, J., Du, W., Qiu, Y., Zhou, W., He, Y., Li, Y., Li, J., Fu, P., Wang, Z., Worsnop, D. R., and Sun, Y.: Summertime aerosol volatility measurements in Beijing, China, Atmospheric Chemistry and Physics, 19, 10205-10216, 10.5194/acp-19-10205-2019, 2019.

1090   Xu, W. Q., Sun, Y. L., Chen, C., Du, W., Han, T. T., Wang, Q. Q., Fu, P. Q., Wang, Z. F., Zhao, X. J., Zhou, L. B., Ji, D. S., Wang, P. C., and Worsnop, D. R.: Aerosol composition, oxidation properties, and sources in Beijing: results from the 2014 Asia-Pacific Economic Cooperation summit study, Atmospheric Chemistry and Physics, 15, 13681-13698, 10.5194/acp-15-13681-2015, 2015.

Yan, Y., Liu, Z., Gao, W., Li, J., Zhang, X., Chai, W., Bai, J., Hu, B., and Wang, Y.: Physiochemistry characteristics and

1095   sources of submicron aerosols at the background area of North China Plain: Implication of air pollution control in heating

season, Atmospheric Research, 249, 10.1016/j.atmosres.2020.105291, 2021.

Yang, S., Yuan, B., Peng, Y., Huang, S., Chen, W., Hu, W., Pei, C., Zhou, J., Parrish, D. D., Wang, W., He, X., Cheng, C., Li,

X. B., Yang, X., Song, Y., Wang, H., Qi, J., Wang, B., Wang, C., Wang, C., Wang, Z., Li, T., Zheng, E., Wang, S., Wu, C.,

Cai, M., Ye, C., Song, W., Cheng, P., Chen, D., Wang, X., Zhang, Z., Wang, X., Zheng, J., and Shao, M.: The formation and

1100   mitigation of nitrate pollution: comparison between urban and suburban environments, Atmos. Chem. Phys., 22, 4539-4556,

10.5194/acp-22-4539-2022, 2022.

Yao, L., Yang, L., Yuan, Q., Yan, C., Dong, C., Meng, C., Sui, X., Yang, F., Lu, Y., and Wang, W.: Sources apportionment of

PM 2.5 in a background site in the North China Plain, Science of The Total Environment, 541, 590-598,

10.1016/j.scitotenv.2015.09.123, 2016.

1105   Yli-Juuti, T., Pajunoja, A., Tikkanen, O. P., Buchholz, A., Faiola, C., Vaisanen, O., Hao, L., Kari, E., Perakyla, O., Garmash,

O., Shiraiwa, M., Ehn, M., Lehtinen, K., and Virtanen, A.: Factors controlling the evaporation of secondary organic aerosol

from alpha-pinene ozonolysis, Geophys Res Lett, 44, 2562-2570, 10.1002/2016GL072364, 2017.

Ylisirniö, A., Buchholz, A., Mohr, C., Li, Z., Barreira, L., Lambe, A., Faiola, C., Kari, E., Yli-Juuti, T., Nizkorodov, S. A.,

Worsnop, D. R., Virtanen, A., and Schobesberger, S.: Composition and volatility of secondary organic aerosol (SOA) formed

1110   from oxidation of real tree emissions compared to simplified volatile organic compound (VOC) systems, Atmospheric

Chemistry and Physics, 20, 5629-5644, 10.5194/acp-20-5629-2020, 2020.

Zhang, J., Wang, Y., Huang, X., Liu, Z., Ji, D., and Sun, Y.: Characterization of organic aerosols in Beijing using an aerodyne

high-resolution aerosol mass spectrometer, Advances in Atmospheric Sciences, 32, 877-888, 10.1007/s00376-014-4153-9,

2015.

1115   Zhang, J. K., Cheng, M. T., Ji, D. S., Liu, Z. R., Hu, B., Sun, Y., and Wang, Y. S.: Characterization of submicron particles

during biomass burning and coal combustion periods in Beijing, China, Sci Total Environ, 562, 812-821,

10.1016/j.scitotenv.2016.04.015, 2016.

Zhang, J. K., Sun, Y., Liu, Z. R., Ji, D. S., Hu, B., Liu, Q., and Wang, Y. S.: Characterization of submicron aerosols during a

month of serious pollution in Beijing, 2013, Atmospheric Chemistry and Physics, 14, 2887-2903, 10.5194/acp-14-2887-

1120   2014, 2014.

Zhang, J. P., Zhu, T., Zhang, Q. H., Li, C. C., Shu, H. L., Ying, Y., Dai, Z. P., Wang, X., Liu, X. Y., Liang, A. M., Shen, H. X.,

and Yi, B. Q.: The impact of circulation patterns on regional transport pathways and air quality over Beijing and its

surroundings, Atmospheric Chemistry and Physics, 12, 5031-5053, 10.5194/acp-12-5031-2012, 2012.

Zhang, Q., Worsnop, D. R., Canagaratna, M. R., and Jimenez, J. L.: Hydrocarbon-like and oxygenated organic aerosols in

1125   Pittsburgh: insights into sources and processes of organic aerosols, Atmos. Chem. Phys., 5, 3289-3311, 10.5194/acp-5-3289-

2005, 2005a.

Zhang, Q., Alfarra, M. R., Worsnop, D. R., Allan, J. D., Coe, H., Canagaratna, M. R., and Jimenez, J. L.: Deconvolution and

Quantification of Hydrocarbon-like and Oxygenated Organic Aerosols Based on Aerosol Mass Spectrometry, Environmental

Science & Technology, 39, 4938-4952, 10.1021/es048568l, 2005b.

1130   Zhang, Q., Jimenez, J. L., Canagaratna, M. R., Ulbrich, I. M., Ng, N. L., Worsnop, D. R., and Sun, Y.: Understanding

atmospheric organic aerosols via factor analysis of aerosol mass spectrometry: a review, Anal Bioanal Chem, 401, 3045-

3067, 10.1007/s00216-011-5355-y, 2011.

Zhang, Q., Jimenez, J. L., Canagaratna, M. R., Allan, J. D., Coe, H., Ulbrich, I., Alfarra, M. R., Takami, A., Middlebrook, A.

M., Sun, Y. L., Dzepina, K., Dunlea, E., Docherty, K., DeCarlo, P. F., Salcedo, D., Onasch, T., Jayne, J. T., Miyoshi, T.,

1135   Shimono, A., Hatakeyama, S., Takegawa, N., Kondo, Y., Schneider, J., Drewnick, F., Borrmann, S., Weimer, S., Demerjian,

K., Williams, P., Bower, K., Bahreini, R., Cottrell, L., Griffin, R. J., Rautiainen, J., Sun, J. Y., Zhang, Y. M., and Worsnop, D.

R.: Ubiquity and dominance of oxygenated species in organic aerosols in anthropogenically-influenced Northern

Hemisphere midlatitudes, Geophysical Research Letters, 34, n/a-n/a, 10.1029/2007gl029979, 2007.

Zhang, R., Jing, J., Tao, J., Hsu, S. C., Wang, G., Cao, J., Lee, C. S. L., Zhu, L., Chen, Z., Zhao, Y., and Shen, Z.: Chemical

1140   characterization and source apportionment ofPM2.5 in Beijing: seasonal perspective, Atmospheric Chemistry and Physics, 13, 7053-7074, 10.5194/acp-13-7053-2013, 2013.

Zhang, Y., Liu, J., Tao, W., Xiang, S., Liu, H., Yi, K., Yang, H., Xu, J., Wang, Y., Ma, J., Wang, X., Hu, J., Wan, Y., Wang, X., and Tao, S.: Impacts of chlorine emissions on secondary pollutants in China, Atmospheric Environment, 10.1016/j.atmosenv.2020.118177, 2020.

1145   Zhang, Y., Sun, J., Zheng, P., Chen, T., Liu, Y., Han, G., Simpson, I. J., Wang, X., Blake, D. R., Li, Z., Yang, X., Qi, Y., Wang, Q., Wang, W., and Xue, L.: Observations of C1-C5 alkyl nitrates in the Yellow River Delta, northern China: Effects of biomass burning and oil field emissions, Sci Total Environ, 656, 129-139, 10.1016/j.scitotenv.2018.11.208, 2019.

Zhang, Y., Du, W., Wang, Y., Wang, Q., Wang, H., Zheng, H., Zhang, F., Shi, H., Bian, Y., Han, Y., Fu, P., Canonaco, F., Prévôt, A. S. H., Zhu, T., Wang, P., Li, Z., and Sun, Y.: Aerosol chemistry and particle growth events at an urban downwind

1150   site in North China Plain, Atmospheric Chemistry and Physics, 18, 14637-14651, 10.5194/acp-18-14637-2018, 2018.

Zhao, J., Du, W., Zhang, Y., Wang, Q., Chen, C., Xu, W., Han, T., Wang, Y., Fu, P., Wang, Z., Li, Z., and Sun, Y.: Insights into aerosol chemistry during the 2015 China Victory Day parade: results from simultaneous measurements at ground level and 260 m in Beijing, Atmospheric Chemistry and Physics, 17, 3215-3232, 10.5194/acp-17-3215-2017, 2017.

Zhao, J., Qiu, Y., Zhou, W., Xu, W., Wang, J., Zhang, Y., Li, L., Xie, C., Wang, Q., Du, W., Worsnop, D. R., Canagaratna, M.

1155   R., Zhou, L., Ge, X., Fu, P., Li, J., Wang, Z., Donahue, N. M., and Sun, Y.: Organic Aerosol Processing During Winter Severe Haze Episodes in Beijing, Journal of Geophysical Research: Atmospheres, 124, 10248-10263, 10.1029/2019jd030832, 2019.

Zhao, Z., Yang, X., Lee, J., Tolentino, R., Mayorga, R., Zhang, W., and Zhang, H.: Diverse Reactions in Highly Functionalized Organic Aerosols during Thermal Desorption, ACS Earth and Space Chemistry, 4, 283-296,

1160   10.1021/acsearthspacechem.9b00312, 2020.

Zheng, G. J., Duan, F. K., Su, H., Ma, Y. L., Cheng, Y., Zheng, B., Zhang, Q., Huang, T., Kimoto, T., Chang, D., Pöschl, U., Cheng, Y. F., and He, K. B.: Exploring the severe winter haze in Beijing: the impact of synoptic weather, regional transport and heterogeneous reactions, Atmospheric Chemistry and Physics, 15, 2969-2983, 10.5194/acp-15-2969-2015, 2015.

Zheng, J., Zhong, L., Wang, T., Louie, P. K. K., and Li, Z.: Ground-level ozone in the Pearl River Delta region: Analysis of

1165   data from a recently established regional air quality monitoring network, Atmospheric Environment, 44, 814-823, 10.1016/j.atmosenv.2009.11.032, 2010.

Zheng, J., Hu, M., Du, Z., Shang, D., Gong, Z., Qin, Y., Fang, J., Gu, F., Li, M., Peng, J., Li, J., Zhang, Y., Huang, X., He, L., Wu, Y., and Guo, S.: Influence of biomass burning from South Asia at a high-altitude mountain receptor site in China, Atmospheric Chemistry and Physics, 17, 6853-6864, 10.5194/acp-17-6853-2017, 2017.

1170   Zheng, P., Chen, T., Dong, C., Liu, Y., Li, H., Han, G., Sun, J., Wu, L., Gao, X., Wang, X., Qi, Y., Zhang, Q., Wang, W., and Xue, L.: Characteristics and sources of halogenated hydrocarbons in the Yellow River Delta region, northern China, Atmos Res, 225, 70-80, https://doi.org/10.1016/j.atmosres.2019.03.039, 2019.

Zhou, S., Collier, S., Xu, J., Mei, F., Wang, J., Lee, Y.-N., Sedlacek, A. J., Springston, S. R., Sun, Y., and Zhang, Q.: Influences of upwind emission sources and atmospheric processing on aerosol chemistry and properties at a rural location in

1175   the Northeastern U.S, Journal of Geophysical Research: Atmospheres, 121, 6049-6065, 10.1002/2015jd024568, 2016.

Zhou, W., Xu, W., Kim, H., Zhang, Q., Fu, P., Worsnop, D. R., and Sun, Y.: A review of aerosol chemistry in Asia: insights from aerosol mass spectrometer measurements, Environ Sci Process Impacts, 22, 1616-1653, 10.1039/d0em00212g, 2020.

Zhou, W., Sun, Y., Xu, W., Zhao, X., Wang, Q., Tang, G., Zhou, L., Chen, C., Du, W., Zhao, J., Xie, C., Fu, P., and Wang, Z.: Vertical Characterization of Aerosol Particle Composition in Beijing, China: Insights From 3-Month Measurements With

1180   Two Aerosol Mass Spectrometers, Journal of Geophysical Research: Atmospheres, 123, 10.1029/2018jd029337, 2018.

Zhu, Q., Cao, L.-M., Tang, M.-X., Huang, X.-F., Saikawa, E., and He, L.-Y.: Characterization of Organic Aerosol at a Rural Site in the North China Plain Region: Sources, Volatility and Organonitrates, Advances in Atmospheric Sciences, 38, 1115-1127, 10.1007/s00376-020-0127-2, 2021.

Zorn, S. R., Drewnick, F., Schott, M., Hoffmann, T., and Borrmann, S.: Characterization of the South Atlantic marine

1185   boundary layer aerosol using an aerodyne aerosol mass spectrometer, Atmos. Chem. Phys., 8, 4711-4728, 10.5194/acp-8-4711-2008, 2008.